

High order numerical simulation of the transmission and scattering of waves using the method of difference potentials [☆]



M. Medvinsky ^{a,b}, S. Tsynkov ^{b,c,*}, E. Turkel ^a

^a School of Mathematical Sciences, Tel Aviv University, Ramat Aviv, Tel Aviv 69978, Israel

^b Department of Mathematics, North Carolina State University, Box 8205, Raleigh, NC 27695, USA

^c Moscow Institute of Physics and Technology, Dolgoprudny 141700, Russia

ARTICLE INFO

Article history:

Received 11 November 2012

Received in revised form 7 March 2013

Accepted 10 March 2013

Available online 22 March 2013

Keywords:

Difference potentials

Boundary projections

Calderon's operators

Regular grids

Curvilinear boundaries

Non-conforming boundaries/interfaces

Variable coefficients

Compact differencing

High order accuracy

Exterior problems

Artificial boundary conditions

ABSTRACT

The method of difference potentials generalizes the method of Calderon's operators from PDEs to arbitrary difference equations and systems. It offers several key advantages, such as the capability of handling boundaries/interfaces that are not aligned with the discretization grid, variable coefficients, and nonstandard boundary conditions. In doing so, the complexity of the algorithm remains comparable to that of an ordinary finite difference scheme on a regular structured grid.

Previously, we have applied the method of difference potentials to solving several variable coefficient interior Helmholtz problems with fourth and sixth order accuracy. We have employed compact finite difference schemes as a core discretization methodology. Those schemes enable high order accuracy on narrow stencils and hence require only as many boundary conditions as needed for the underlying differential equation itself. Numerical experiments corroborate the high order accuracy of our method for variable coefficients, regular grids, and non-conforming boundaries.

In the current paper, we extend the previously developed methodology to exterior problems. We present a complete theoretical analysis of the algorithm, as well as the results of a series of numerical simulations. Specifically, we study the scattering of time-harmonic waves about smooth shapes, subject to various boundary conditions. We also solve the transmission/scattering problems, in which not only do the waves scatter off a given shape but also propagate through the interface and travel across the heterogeneous medium inside. In all the cases, our methodology guarantees high order accuracy for regular grids and non-conforming boundaries and interfaces.

© 2013 Elsevier Inc. All rights reserved.

1. Introduction

1.1. Formulation of the problem

This paper focuses on the high order numerical simulation of the transmission and scattering of time-harmonic waves about compactly supported smooth shapes with variable material properties inside and constant material characteristics

[☆] Work supported by the US NSF under Grant # DMS-0810963, by the US–Israel Binational Science Foundation (BSF) under Grant # 2008094, and by the US ARO under Grant # W911NF-11-1-0384.

* Corresponding author at: Department of Mathematics, North Carolina State University, Box 8205, Raleigh, NC 27695, USA. Tel.: +1 919 515 1877.

E-mail addresses: medvinsk@post.tau.ac.il (M. Medvinsky), tsynkov@math.ncsu.edu (S. Tsynkov), turkel@post.tau.ac.il (E. Turkel).

URLs: <http://www.tau.ac.il/~medvinsk/> (M. Medvinsky), <http://www.math.ncsu.edu/~stsynkov> (S. Tsynkov), <http://www.math.tau.ac.il/~turkel/> (E. Turkel).

outside. Let Ω be a bounded domain, $\Omega \subset \mathbb{R}^2$, with a smooth boundary $\Gamma = \partial\Omega$, see Fig. 1. Let $u = u(\mathbf{x})$, $\mathbf{x} \in \mathbb{R}^2$, denote the unknown complex-valued scalar time-harmonic wave field (e.g., acoustic or linearly polarized electromagnetic) governed by an inhomogeneous variable coefficient Helmholtz equation inside Ω :

$$\mathbf{L}_1 u \equiv \Delta u + k_1^2 u = f \tag{1a}$$

and the homogeneous constant coefficient Helmholtz equation outside Ω , i.e., on $\tilde{\Omega} \stackrel{\text{def}}{=} \mathbb{R}^2 \setminus \bar{\Omega}$:

$$\mathbf{L}_0 u \equiv \Delta u + k_0^2 u = 0. \tag{1b}$$

For the pure exterior problem we have Eq. (1b) and a boundary condition on Γ . In Eq. (1a), the wavenumber $k_1 = k_1(\mathbf{x})$ and the right-hand side $f = f(\mathbf{x})$ are given sufficiently smooth functions of $\mathbf{x} \in \Omega$. The wavenumber k_0 in Eq. (1b) is constant on $\tilde{\Omega}$, and the overall wavenumber $k = k(\mathbf{x})$, which is defined on the entire \mathbb{R}^2 by the formula

$$k(\mathbf{x}) = \begin{cases} k_1(\mathbf{x}), & \mathbf{x} \in \Omega, \\ k_0 = \text{const}, & \mathbf{x} \in \tilde{\Omega}, \end{cases} \tag{2}$$

can undergo a jump discontinuity at the interface Γ , see Fig. 1.

In addition to the source term f of Eq. (1a), the excitation in the problem may be provided by the given incident field, $u^{(\text{inc})} = u^{(\text{inc})}(\mathbf{x})$, $\mathbf{x} \in \tilde{\Omega}$, which itself is required to satisfy the homogeneous Helmholtz equation (1b). With no loss of generality, we take $u^{(\text{inc})}$ as a plane wave:

$$u^{(\text{inc})}(\mathbf{x}) = u_0 e^{ik_0(x_1 \cos \theta + x_2 \sin \theta)}, \tag{3}$$

where $\mathbb{R}^2 \supset \tilde{\Omega} \ni \mathbf{x} = (x_1, x_2)$, and θ is the angle of incidence, see Fig. 1. The total field u on the exterior domain $\tilde{\Omega}$ is partitioned into the incident and scattered components:

$$u(\mathbf{x}) = u^{(\text{inc})}(\mathbf{x}) + u^{(\text{sc})}(\mathbf{x}), \quad \mathbf{x} \in \tilde{\Omega}. \tag{4}$$

Since both the total field u and the incident field $u^{(\text{inc})}$ of (4) satisfy the homogeneous equation (1b), so does the scattered field $u^{(\text{sc})}$. In addition, we require that the scattered field satisfy the two-dimensional Sommerfeld radiation condition at infinity:

$$\lim_{r \rightarrow \infty} \sqrt{r} \left(\frac{\partial u^{(\text{sc})}}{\partial r} + ik_0 u^{(\text{sc})} \right) = 0, \quad \text{where } r \equiv |\mathbf{x}|. \tag{5}$$

Conversely, the incident field $u^{(\text{inc})}$ should not satisfy (5) (see, e.g., (3)); otherwise, it would be indistinguishable from the scattered field $u^{(\text{sc})}$ and would provide no excitation to the problem.

Finally, the wavenumber $k(\mathbf{x})$ of (2) may be discontinuous across Γ , special interface conditions are required. In the simplest case, they reduce to the continuity of the solution u and its first normal derivative on Γ :

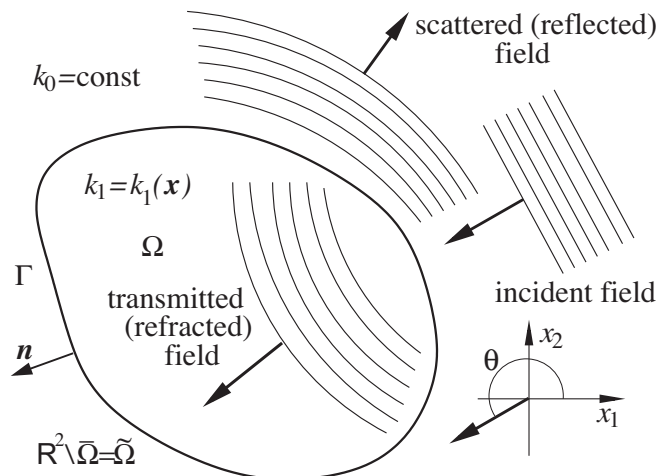


Fig. 1. Schematic for the transmission/scattering problem.

$$u^{(\Omega)}|_{\Gamma} = u^{(\tilde{\Omega})}|_{\Gamma}, \quad \frac{\partial u^{(\Omega)}}{\partial \mathbf{n}}|_{\Gamma} = \frac{\partial u^{(\tilde{\Omega})}}{\partial \mathbf{n}}|_{\Gamma}. \tag{6}$$

In (6), \mathbf{n} is the outward normal to Γ , and the superscripts “ (Ω) ” and “ $(\tilde{\Omega})$ ” denote the interior and exterior side of Γ , respectively. Other interface conditions may also be considered, see (20).

The overall problem (1), (4)–(6) is required to have a unique solution u for a given right-hand side f and a given incident field $u^{(\text{inc})}$, e.g., the plane wave (3). The formulation is also assumed to be well-posed. The proof for $k_1 = \text{const}$ can be found, e.g., in [1, Chapter VII]. The problem setting that we have described is typical for many applications ranging from medical imaging to underwater acoustics to land mine detection.

1.2. Bibliography notes

The problem formulated in Section 1.1 will be solved using Calderon’s operators and the method of difference potentials. Its key advantages are the capability of treating the non-conforming boundaries and variable coefficients on regular structured grids with no loss of accuracy and no need of evaluating singular integrals.

In the literature, Calderon’s operators were first introduced by Calderon [2] and then studied by Seeley [3]. The fundamentals of the method difference potentials are presented in the review paper [4] and monograph [5] by Ryaben’kii. In our work [6], we provide a thorough description of the method of difference potentials as it applies to solving interior problems for the variable coefficient Helmholtz equation approximated by compact schemes with high order accuracy. An earlier application of the method of difference potentials to problems on composite domains is reported in [7], and an earlier application to exterior scattering problems (about bodies of revolution) is presented in [8]. In both cases the computations were performed with second order accuracy. Other developments of the method can be found, e.g., in [9–15].

1.3. Calderon’s operators

We now describe the method with the extension to the exterior and combined exterior–interior problems. First, consider a larger domain Ω_1 such that $\Omega \subseteq \Omega_1 \subseteq \mathbb{R}^2$. Taking a sufficiently smooth extension of the function $k_1(\mathbf{x})$ from Ω to Ω_1 , we define the operator \mathbf{L}_1 of (1a) on Ω_1 . Let U_1 and F_1 be two spaces of functions on Ω_1 , $\mathbf{L}_1 : U_1 \mapsto F_1$. The space U_1 must be characterized by a certain degree of regularity sufficient for applying the operator \mathbf{L}_1 in the classical sense, and the inclusion $u \in U_1$ should also imply that $u(\mathbf{x})$ satisfies a certain auxiliary boundary condition at $\partial\Omega_1$. The regularity of the functions from F_1 must be commensurate with that of the functions from U_1 in the sense that $F_1 \subset \text{Im}\mathbf{L}_1$, and we additionally require that if $f \in F_1$ then also $\chi_{\Omega}f \in F_1$, where χ_{Ω} is the indicator function of Ω , i.e., $\chi_{\Omega}(\mathbf{x}) = 1$ for $\mathbf{x} \in \Omega$ and $\chi_{\Omega}(\mathbf{x}) = 0$ for $\mathbf{x} \in \Omega_1 \setminus \Omega$.

Next, let Ω_1 , U_1 , and F_1 be chosen so that the Helmholtz equation (1a) has a unique solution $u \in U_1$ on Ω_1 for any $f \in F_1$. Hereafter, we will refer to solving Eq. (1a) on Ω_1 in the class of functions U_1 as to solving the interior auxiliary problem (AP). Given $f \in F_1$, we will denote the corresponding solution by $u = \mathbf{G}_1f$, where $\mathbf{G}_1 : F_1 \mapsto U_1$ is the Green’s (i.e., inverse) operator of this AP. We additionally assume that the interior AP we have just described is well-posed.

For a given $v = v(\mathbf{x})$, $\mathbf{x} \in \Omega$, introduce its vector boundary trace at the interior side of Γ :

$$\mathbf{Tr}_1 v \stackrel{\text{def}}{=} \left(v^{(\Omega)}, \frac{\partial v^{(\Omega)}}{\partial \mathbf{n}} \right) \Big|_{\Gamma}. \tag{7}$$

Let $\xi_{\Gamma} = (\xi_0, \xi_1)$ be a vector function with two components defined on Γ . Choose an auxiliary function $w \in U_1$ on Ω_1 such that $\mathbf{Tr}_1 w = \xi_{\Gamma}$ in the sense of (7). The generalized Calderon potential with density ξ_{Γ} is defined as follows:

$$\mathbf{P}_{\Omega}\xi_{\Gamma}(\mathbf{x}) \stackrel{\text{def}}{=} w(\mathbf{x}) - \mathbf{G}_1[\chi_{\Omega}\mathbf{L}_1 w](\mathbf{x}), \quad \mathbf{x} \in \Omega. \tag{8}$$

Clearly, $\mathbf{L}_1\mathbf{P}_{\Omega}\xi_{\Gamma}(\mathbf{x}) = 0$ on Ω . The generalized Calderon projection is the trace of the potential (8):

$$\mathbf{P}_{\Gamma,1}\xi_{\Gamma} \stackrel{\text{def}}{=} \mathbf{Tr}_1\mathbf{P}_{\Omega}\xi_{\Gamma}. \tag{9}$$

A given $u = u(\mathbf{x})$, $\mathbf{x} \in \Omega$, provides a solution to the Helmholtz equation (1a) in Ω if and only if its trace (7), $\xi_{\Gamma}^{(\Omega)} = \mathbf{Tr}_1 u$, satisfies the Calderon boundary equation with projection (BEP):

$$\mathbf{P}_{\Gamma,1}\xi_{\Gamma}^{(\Omega)} + \mathbf{Tr}_1\mathbf{G}_1f = \xi_{\Gamma}^{(\Omega)}. \tag{10}$$

In formula (10), it is assumed the right-hand side f of Eq. (1a) is defined only on Ω : $\text{supp}f \subseteq \Omega$. If the BEP (10) holds, then the corresponding solution of Eq. (1a) is given by

$$u(\mathbf{x}) = \mathbf{P}_{\Omega}\xi_{\Gamma}^{(\Omega)}(\mathbf{x}) + \mathbf{G}_1f(\mathbf{x}), \quad \mathbf{x} \in \Omega. \tag{11}$$

Similarly, consider another auxiliary domain, $\tilde{\Omega}_0$, such that $\tilde{\Omega} \subseteq \tilde{\Omega}_0 \subseteq \mathbb{R}^2$, and two spaces of functions, U_0 and F_0 , defined on $\tilde{\Omega}_0$, $\mathbf{L}_0 : U_0 \mapsto F_0$, where \mathbf{L}_0 is the constant coefficient Helmholtz operator of (1b). The same considerations of regularity that

apply to U_1 and F_1 pertain to U_0 and F_0 as well, and in addition, we require that the functions $u \in U_0$ satisfy the Sommerfeld condition (5) along with some auxiliary boundary condition at $\partial\tilde{\Omega}_0$ needed when $\partial\tilde{\Omega}_0 \neq \emptyset$. The problem of solving Eq. (1b) on $\tilde{\Omega}_0$ in the space U_0 will be referred to as the exterior AP. We assume that it has a unique solution $u \in U_0$ for any $f \in F_0$, and that it is well-posed. The solution will be denoted by $u = \mathbf{G}_0 f$, where $\mathbf{G}_0 : F_0 \mapsto U_0$ is the Green’s operator of the exterior AP.

For a given $v = v(\mathbf{x})$ on $\tilde{\Omega}$, we introduce its boundary trace on the exterior side of Γ (cf. (7)):

$$\mathbf{Tr}_0 v \stackrel{\text{def}}{=} \left(v^{(\tilde{\Omega})}, \frac{\partial v^{(\tilde{\Omega})}}{\partial \mathbf{n}} \right) \Big|_{\Gamma}. \tag{12}$$

Note, that for defining the interior trace (7) and the exterior trace (12) we need the differentiability of $v(\mathbf{x})$ all the way up to the interface Γ from the interior and exterior side, respectively,¹ but we do not necessarily need the regularity of $v(\mathbf{x})$ across the interface. In fact, in each of the two individual cases, (7) or (12), the corresponding $v(\mathbf{x})$ does not even have to be known beyond Γ .

The generalized Calderon potential and projection for the exterior domain $\tilde{\Omega}$ are defined similarly to those for the interior domain Ω . Let $\xi_\Gamma = (\xi_0, \xi_1)$ be a two-component vector function on Γ . Take an auxiliary function $w \in U_0$ on $\tilde{\Omega}_0$ such that $\mathbf{Tr}_0 w = \xi_\Gamma$ in the sense of (12). The exterior generalized Calderon potential with density ξ_Γ is defined as follows (cf. formula (8)):

$$\mathbf{P}_{\tilde{\Omega}} \xi_\Gamma(\mathbf{x}) \stackrel{\text{def}}{=} w(\mathbf{x}) - \mathbf{G}_0[\chi_{\tilde{\Omega}} \mathbf{L}_0 w](\mathbf{x}), \quad \mathbf{x} \in \tilde{\Omega}. \tag{13}$$

In formula (13), $\chi_{\tilde{\Omega}} = \chi_{\tilde{\Omega}}(\mathbf{x})$ is the characteristic function of the domain $\tilde{\Omega}$, i.e., $\chi_{\tilde{\Omega}}(\mathbf{x}) = 1$ if $\mathbf{x} \in \tilde{\Omega}$ and $\chi_{\tilde{\Omega}}(\mathbf{x}) = 0$ if $\mathbf{x} \in \tilde{\Omega}_0 \setminus \tilde{\Omega}$. It is easy to see that $\mathbf{L}_0 \mathbf{P}_{\tilde{\Omega}} \xi_\Gamma(\mathbf{x}) = 0$ on $\tilde{\Omega}$. The exterior generalized Calderon projection is the trace of the exterior potential (13) (cf. formula (9)):

$$\mathbf{P}_{\Gamma,0} \xi_\Gamma \stackrel{\text{def}}{=} \mathbf{Tr}_0 \mathbf{P}_{\tilde{\Omega}} \xi_\Gamma. \tag{14}$$

A solution to the Helmholtz equation (1b) on $\tilde{\Omega}$ subject to the radiation condition (5) is referred to as the scattering solution, see Fig. 1. A given $u^{(\text{sc})} = u^{(\text{sc})}(\mathbf{x})$, $\mathbf{x} \in \tilde{\Omega}$, satisfies (1b) and (5) on $\tilde{\Omega}$ if and only if its trace (12), $\xi_\Gamma^{(\tilde{\Omega},\text{sc})} = \mathbf{Tr}_0 u^{(\text{sc})}$, solves the exterior BEP:

$$\mathbf{P}_{\Gamma,0} \xi_\Gamma^{(\tilde{\Omega},\text{sc})} = \xi_\Gamma^{(\tilde{\Omega},\text{sc})}. \tag{15}$$

Unlike the interior BEP (10), the BEP (15) is homogeneous, because Eq. (1b) is homogeneous. If the BEP (15) holds, then the corresponding scattering solution of Eq. (1b) is given by the potential (13):

$$u^{(\text{sc})}(\mathbf{x}) = \mathbf{P}_{\tilde{\Omega}} \xi_\Gamma^{(\tilde{\Omega},\text{sc})}(\mathbf{x}), \quad \mathbf{x} \in \tilde{\Omega}. \tag{16}$$

The overall exterior solution on $\tilde{\Omega}$ is a superposition of the incident and scattered fields, see formula (4). Let us then add $\xi_\Gamma^{(\text{inc})} \equiv \mathbf{Tr}_0 u^{(\text{inc})}$ to both sides of equality (15), which yields: $\mathbf{P}_{\Gamma,0} \xi_\Gamma^{(\tilde{\Omega},\text{sc})} + \xi_\Gamma^{(\text{inc})} = \xi_\Gamma^{(\tilde{\Omega})}$. If we also replace the trace of the scattered field $\xi_\Gamma^{(\tilde{\Omega},\text{sc})}$ by the overall trace $\xi_\Gamma^{(\tilde{\Omega})} = \mathbf{Tr}_0 u$ under the projection $\mathbf{P}_{\Gamma,0}$, then we arrive at the following result.

For a given $u^{(\text{inc})} = u^{(\text{inc})}(\mathbf{x})$, $\mathbf{L}_0 u^{(\text{inc})} = 0$ for $\mathbf{x} \in \tilde{\Omega}$, the function $u(\mathbf{x}) = u^{(\text{inc})}(\mathbf{x}) + u^{(\text{sc})}(\mathbf{x})$ satisfies Eq. (1b) on $\tilde{\Omega}$ while at the same time $u^{(\text{sc})}$ satisfies (5) if and only if the trace $\xi_\Gamma^{(\tilde{\Omega})} = \mathbf{Tr}_0 u$ satisfies the inhomogeneous exterior BEP (cf. formula (10)):

$$\mathbf{P}_{\Gamma,0} \xi_\Gamma^{(\tilde{\Omega})} + (\mathbf{I} - \mathbf{P}_{\Gamma,0}) \xi_\Gamma^{(\text{inc})} = \xi_\Gamma^{(\tilde{\Omega})}, \tag{17}$$

where \mathbf{I} is the identity operator in the space of functions $\xi_\Gamma = (\xi_0, \xi_1)$. Note that if $u^{(\text{inc})} \in U_0$, which could be the case if the incident field were generated by the sources $f^{(\text{inc})} \in F_0$ located on $\tilde{\Omega}$, then $\mathbf{P}_{\Gamma,0} \xi_\Gamma^{(\text{inc})} = 0$. Hence, BEP (17) reduces to $\mathbf{P}_{\Gamma,0} \xi_\Gamma^{(\tilde{\Omega})} + \xi_\Gamma^{(\text{inc})} = \xi_\Gamma^{(\tilde{\Omega})}$, which is equivalent to (10). For the plane wave (3) though, we generally have $\mathbf{P}_{\Gamma,0} \xi_\Gamma^{(\text{inc})} \neq 0$ because $u^{(\text{inc})}$ of (3) does not satisfy the Sommerfeld radiation condition (5). Therefore, Eq. (17) stays the way it is.

If the BEP (17) holds, then the overall exterior solution is given by (cf. formula (11))

$$u(\mathbf{x}) = \mathbf{P}_{\tilde{\Omega}}[\xi_\Gamma^{(\tilde{\Omega})} - \xi_\Gamma^{(\text{inc})}](\mathbf{x}) + u^{(\text{inc})}(\mathbf{x}), \quad \mathbf{x} \in \tilde{\Omega}. \tag{18}$$

We emphasize that the Calderon boundary representations (10) and (17) are equivalent to the interior and exterior sub-problems, respectively, of the overall transmission/scattering problem described in Section 1.1. It is very important that this equivalence is not contingent on any particular type of the boundary or interface conditions at Γ . This is in contradistinction to the classical method of boundary integral equations (BIE).

Once we have obtained the BEPs (10) and (17), reducing the overall transmission/scattering problem of Section 1.1 from \mathbb{R}^2 to the interface Γ becomes straightforward. All we have to do is realize that the interface conditions (6) can be recast as follows:

$$\xi_\Gamma^{(\tilde{\Omega})} = \xi_\Gamma^{(\tilde{\Omega})}. \tag{19}$$

¹ More precisely, what is required is the existence of the so-called proper normal derivative [16] of $v(\mathbf{x})$, i.e., a uniform limit of the normal derivative, from inside Γ or from outside Γ .

Then, Eqs. (10), (17), and (19) will be solved as a system, after which the solution on Ω and $\tilde{\Omega}$ can be reconstructed using formulae (11) and (18), respectively. Moreover, one can consider alternative interface conditions as well. Instead of (19), we have a more general relation

$$\mathbf{A}\xi_{\Gamma}^{(\Omega)} + \mathbf{B}\xi_{\Gamma}^{(\tilde{\Omega})} + \boldsymbol{\varphi} = \mathbf{0}, \quad (20)$$

where \mathbf{A} and \mathbf{B} are operators and $\boldsymbol{\varphi}$ represents the boundary data. Eq. (20) will be considered as a part of the overall system along with the BEPs (10) and (17), to be solved with respect to $\xi_{\Gamma}^{(\Omega)}$ and $\xi_{\Gamma}^{(\tilde{\Omega})}$. Note that formula (20) reduces to (19) when $\mathbf{A} = \mathbf{I}$, $\mathbf{B} = -\mathbf{I}$, and $\boldsymbol{\varphi} = \mathbf{0}$.

1.4. Overview of the features

Calderon's operators offer a very general approach to the treatment of the boundary and/or interface conditions. The BEP characterizes the entire class of solutions for a given differential equation (or system) on a given region, without any boundary conditions being involved. The boundary and/or interface conditions complement the BEP(s), and in doing so basically any type of those conditions is allowed (mixed, nonlocal, etc.).

The resulting boundary problem, which consists of the BEP(s) and the boundary/interface conditions, is always well-posed as long as the original boundary value problem is well-posed [5]. This automatic well-posedness, along with the generality and ease in handling the boundary conditions, contrasts with the difficulties arising for BIE. In BIE, a given boundary value problem, rather than only the governing equation(s), is reduced from the domain to the boundary. In doing so, the boundary condition essentially determines the way it is done. For example, to maintain well-posedness of the boundary representation, i.e., to obtain a Fredholm integral equation of the second kind, as opposed to the first kind, a double layer potential should be used for the Dirichlet boundary condition, and a single layer potential should be used for the Neumann boundary condition.

Another important improvement compared with BIE is the ability of Calderon's operators to handle variable coefficients or equivalently, heterogeneous media. The definition and key properties of Calderon's potentials and projections for variable coefficients are the same as those for constant coefficients. The only component that may change is the Green's (inverse) operator of the AP.

The discrete counterparts of Calderon's potentials and projections are obtained in the framework of the method of difference potentials, see Section 2. This method applies to any finite difference scheme. In particular, the scheme can be built on a regular grid for convenience, while the boundaries/interfaces need not necessarily conform to the grid. For example, compact high order schemes of type [17–19] offer a very economical venue for obtaining high order accuracy (compared to some high order finite elements). In doing so, non-conforming boundaries result in no deterioration of accuracy if handled by the method of difference potentials.

Numerical computation of the discrete Calderon potentials and projections involves solving the AP(s) by finite differences, and the corresponding inverse (Green's) operators are obtained without having to evaluate singular integrals. This is another important improvement compared with BIE.

1.5. Outline of the paper

The rest of the paper is organized as follows. In Section 2, we describe the constructs of the method of difference potentials as it applies to solving the transmission/scattering problem formulated in Section 1.1. Specifically, in Section 2.1 we build the discrete Calderon potentials and projections for the interior subproblem and in Section 2.2 we construct the discrete Calderon potentials and projections for the exterior subproblem. In Section 2.3, we apply the interface conditions and match the solutions of the two subproblems at Γ . In Section 3, we present the results of our numerical simulations that corroborate the theoretical design properties of the proposed algorithm. In Section 4, we draw some conclusions, and also discuss future work.

2. Discrete Calderon's operators

For ease of implementation, we approximate the interior subproblem on a Cartesian grid, and the exterior subproblem on a polar grid. Their solutions will be matched at the interface Γ .

2.1. Interior subproblem

Let the auxiliary domain Ω_1 introduced in Section 1.3 be a rectangle that contains Ω , see Fig. 2, and let \mathbb{N}_1 be uniform in each direction of a Cartesian grid in this rectangle. We approximate Eq. (1a) (with its variable wavenumber $k_1 = k_1(\mathbf{x})$ extended smoothly from Ω to $\Omega_1 \supset \Omega$) on the grid \mathbb{N}_1 by the compact fourth order accurate² finite difference scheme [18] that we express schematically as

² The sixth order accurate scheme of [19] can also be used.

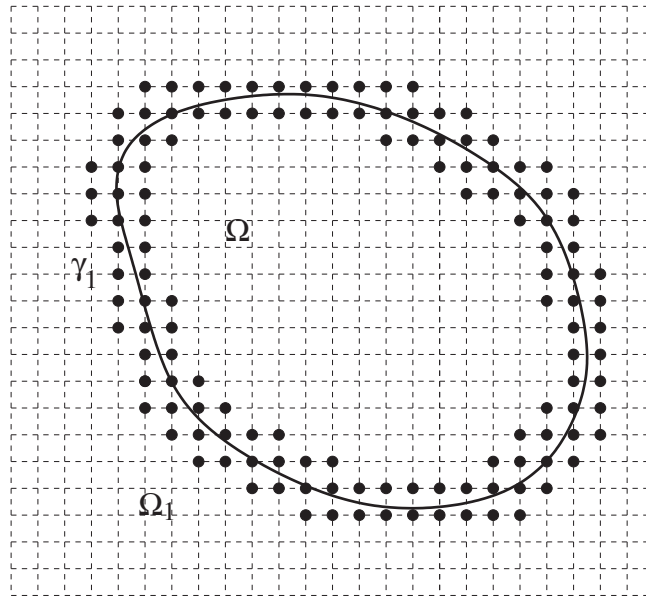


Fig. 2. Computational domain, grid, and the grid boundary γ_1 for the interior subproblem.

$$\mathbf{L}_1^{(h)} u = \mathbf{B}_1^{(h)} \bar{f}. \tag{21}$$

In formula (21), $u \in \mathcal{U}_1$ denotes the discrete solution on \mathbb{N}_1 , and \bar{f} is the discrete right-hand side, i.e., a representation of the right-hand side $f(\mathbf{x})$ on the grid. The discrete operators $\mathbf{L}_1^{(h)}$ and $\mathbf{B}_1^{(h)}$ in (21) are built on a 9-point 3×3 stencil and a 5-point central difference stencil, respectively. Accordingly, both the left-hand side and the right-hand side of Eq. (21) are defined only on the interior sub-grid \mathbb{M}_1 of the grid \mathbb{N}_1 , such that $\mathbb{N}_1 \setminus \mathbb{M}_1 \subset \partial\Omega_1$. So, \mathbb{M}_1 excludes all the nodes of \mathbb{N}_1 that happen to lie exactly on the boundary of the rectangle Ω_1 . We require that all functions from the space of solutions \mathcal{U}_1 satisfy a certain auxiliary boundary condition on $\partial\Omega_1$ (i.e., at $\mathbb{N}_1 \setminus \mathbb{M}_1$) so that for any $g = \mathbf{B}_1^{(h)} \bar{f}$ there exists a unique solution $u \in \mathcal{U}_1$ of the finite difference equation (21). We denote this solution by $u = \mathbf{G}_1^{(h)} g$, where $\mathbf{G}_1^{(h)}$ is the discrete Green's operator, i.e., an inverse to $\mathbf{L}_1^{(h)}$ subject to $u \in \mathcal{U}_1$. The problem of finding the solution $u \in \mathcal{U}_1$ to the equation $\mathbf{L}_1^{(h)} u = g$ for a given g will be referred to as the discrete interior AP.

The operator $\mathbf{L}_1^{(h)}$ of the compact scheme (21) plays a central role in constructing the discrete counterparts of Calderon's operators. Denote by \mathbb{N}_m the 9-point stencil of the operator $\mathbf{L}_1^{(h)}$ centered around the node $m \equiv (i, j) \in \mathbb{M}_1$:

$$\mathbb{N}_m \equiv \mathbb{N}_{(i,j)} = \{(i, j), (i \pm 1, j), (i, j \pm 1), (i + 1, j + 1), (i + 1, j - 1), (i - 1, j + 1), (i - 1, j - 1)\}. \tag{22}$$

Next, partition the nodes of the grid \mathbb{M}_1 into two subsets:

$$\mathbb{M}_1^+ = \mathbb{M}_1 \cap \bar{\Omega} \quad \text{and} \quad \mathbb{M}_1^- = \mathbb{M}_1 \cap \{\Omega_1 \setminus \bar{\Omega}\} \tag{23a}$$

so that $\mathbb{M}_1^+ \cup \mathbb{M}_1^- = \mathbb{M}_1$ and $\mathbb{M}_1^+ \cap \mathbb{M}_1^- = \emptyset$. Then, we define the subsets \mathbb{N}_1^+ and \mathbb{N}_1^- of the grid \mathbb{N}_1 by applying the stencil \mathbb{N}_m of (22) to each node of \mathbb{M}_1^+ and \mathbb{M}_1^- , respectively:

$$\mathbb{N}_1^+ = \bigcup_{m \in \mathbb{M}_1^+} \mathbb{N}_m, \quad \mathbb{N}_1^- = \bigcup_{m \in \mathbb{M}_1^-} \mathbb{N}_m. \tag{23b}$$

While the sets \mathbb{M}_1^+ and \mathbb{M}_1^- do not overlap, the sets \mathbb{N}_1^+ and \mathbb{N}_1^- obviously do, and their intersection is called the interior grid boundary:

$$\gamma_1 \stackrel{\text{def}}{=} \mathbb{N}_1^+ \cap \mathbb{N}_1^-. \tag{23c}$$

It is a multi-layer fringe of grid nodes that straddles the continuous boundary Γ , as is shown schematically in Fig. 2. The density of the difference potential, which is a discrete counterpart of the Calderon potential (8), will be defined on the grid boundary γ_1 .

Let ξ_{γ_1} be a grid function defined on γ_1 . Take an arbitrary $w \in \mathcal{U}_1$ such that

$$\mathbf{T}_1^{(h)} w \stackrel{\text{def}}{=} w|_{\gamma_1} = \xi_{\gamma_1}$$

and introduce the interior difference potential with the density ξ_{γ_1} (cf. formula (8)):

$$\mathbf{P}_{\mathbb{N}_1^+} \xi_{\gamma_1} \stackrel{\text{def}}{=} w - \mathbf{G}_1^{(h)} \left(\chi_{\mathbb{M}_1^+} \mathbf{L}_1^{(h)} w \right) \quad \text{on the grid } \mathbb{N}_1^+. \tag{24}$$

In formula (24), $\chi_{\mathbb{M}_1^+} = 1$ on the grid \mathbb{M}_1^+ and $\chi_{\mathbb{M}_1^+} = 0$ elsewhere on \mathbb{M}_1 . It can be shown [5] that the potential $\mathbf{P}_{\mathbb{N}_1^+} \xi_{\gamma_1}$ of (24) is insensitive to the choice of $w \in \mathbb{U}_1$ as long as $\mathbf{Tr}_1^{(h)} w = \xi_{\gamma_1}$, and

$$\mathbf{L}_1^{(h)} \left[\mathbf{P}_{\mathbb{N}_1^+} \xi_{\gamma_1} \right] = 0 \quad \text{on the grid } \mathbb{M}_1^+. \tag{25}$$

In doing so, we note that the source function $g = \chi_{\mathbb{M}_1^+} \mathbf{L}_1^{(h)} w$, to which the Green's operator $\mathbf{G}_1^{(h)}$ of the discrete interior AP is applied in formula (24), is a special source function which does not necessarily have to be represented in the form $\mathbf{B}_1^{(h)} \bar{f}$.

The discrete interior boundary projection is the trace of the potential (24) on γ_1 (cf. (9)):

$$\mathbf{P}_{\gamma_1} \xi_{\gamma_1} \stackrel{\text{def}}{=} \mathbf{Tr}_1^{(h)} \mathbf{P}_{\mathbb{N}_1^+} \xi_{\gamma_1}. \tag{26}$$

A given ξ_{γ_1} satisfies the discrete interior BEP (cf. formula (10))

$$\mathbf{P}_{\gamma_1} \xi_{\gamma_1} + \mathbf{Tr}_1^{(h)} \mathbf{G}_1^{(h)} \mathbf{B}_1^{(h)} \bar{f} = \xi_{\gamma_1} \tag{27}$$

if and only if there exists a function u on the grid \mathbb{N}_1^+ that solves the difference equation (21) on the grid \mathbb{M}_1^+ and such that $\mathbf{Tr}_1^{(h)} u = \xi_{\gamma_1}$. If the BEP (27) holds, then the corresponding solution u on \mathbb{N}_1^+ is given by the discrete generalized Green's formula (cf. formula (11)):

$$u = \mathbf{P}_{\mathbb{N}_1^+} \xi_{\gamma_1} + \mathbf{G}_1^{(h)} \mathbf{B}_1^{(h)} \bar{f}. \tag{28}$$

Hence, the discrete interior BEP (27) equivalently reduces the finite difference equation (21) that approximates the differential equation (1a) on Ω , from its grid domain \mathbb{N}_1^+ to the grid boundary γ_1 . The BEP (27) itself has multiple solutions as so does Eq. (21) as well as Eq. (1a). The solution becomes unique when the interior subproblem is coupled with the exterior subproblem. At the continuous level, the coupling is rendered by the interface conditions (6) or, more generally, (20). At the discrete level, the coupling is discussed in Section 2.3.

We emphasize that the right-hand side operator $\mathbf{B}_1^{(h)}$ of the compact scheme (21) plays no role in constructing the difference potential (24). Indeed, the continuous potential (8) satisfies the homogeneous equation $\mathbf{L}_1 \mathbf{P}_\Omega \xi_r(\mathbf{x}) = 0$ on Ω . Likewise, the difference potential (24) satisfies the discrete homogeneous equation (25) on \mathbb{M}_1^+ . The scheme (21) applied to a homogeneous equation $\mathbf{L}_1 u = 0$ transforms into $\mathbf{L}_1^{(h)} u = 0$. Hence, the operator $\mathbf{B}_1^{(h)}$ is not needed for approximating the solutions to the homogeneous equations and accordingly, it does not appear in formula (24). Yet in the full inhomogeneous formulation, the contribution of the right-hand side $f(\mathbf{x})$ of Eq. (1a) enters into the discrete BEP (27), as well as into the discrete Green's formula (28), via $\mathbf{B}_1^{(h)} \bar{f}$.

2.2. Exterior subproblem

Let the auxiliary domain $\tilde{\Omega}_0$ introduced in Section 1.3 be the exterior of a circle of radius $r = R_0$ completely contained inside Γ , see Fig. 3. Let \mathbb{N}_0 be a uniform, in each direction, polar grid on the domain $\tilde{\Omega}_0$. We approximate Eq. (1b) on the grid \mathbb{N}_0 by the compact fourth order accurate finite difference scheme of [17] that we write schematically as

$$\mathbf{L}_0^{(h)} u = 0. \tag{29}$$

Similar to the operator $\mathbf{L}^{(h)}$ of (21), the discrete operator $\mathbf{L}_0^{(h)}$ in formula (29) is also built on a 9-point 3×3 stencil. Moreover, as the domain $\tilde{\Omega}_0$ is unbounded, it is truncated by a larger circle of radius $r = R_1$, see Fig. 3, for the purpose of obtaining a finite-dimensional discrete approximation. In doing so, an artificial boundary condition (ABC) is required at the outer boundary $r = R_1$.

Recall that the overall exterior solution u is a superposition of the incident and scattered fields (cf. formula (4)):

$$u = u^{(\text{inc})} + u^{(\text{sc})}, \tag{30}$$

where $u^{(\text{inc})}$ is given. For the scattered field $u^{(\text{sc})}$, we specify an exact nonlocal ABC at the outer boundary $r = R_1$, which is equivalent to the Sommerfeld condition at infinity (5). The ABC that we use is obtained in Fourier space after the separation of variables. It is approximated on the polar grid with fourth order accuracy using compact finite differences, see [17]. Alternatively, one can use any sufficiently accurate approximation to the Sommerfeld radiation condition (5), see, e.g. [20].

The discrete exterior AP is formulated for the inhomogeneous counterpart of Eq. (29):

$$\mathbf{L}_0^{(h)} u = g \tag{31}$$

subject to the ABC introduced at $r = R_1$. Its solution $u \in \mathbb{U}_0$ is defined on the grid \mathbb{N}_0 , and the right-hand side g is defined on its sub-grid \mathbb{M}_0 , which excludes those nodes of \mathbb{N}_0 that lie either on the inner circle $r = R_0$ or on the outer circle $r = R_1$, see Fig. 3:

$$\mathbb{N}_0 \setminus \mathbb{M}_0 \subset \partial \tilde{\Omega}_0 \equiv \{r = R_0 \cup r = R_1\}.$$

We require that, in addition to the ABC at the outer boundary $r = R_1$, each function u from the space of solutions \mathbb{U}_0 to the discrete exterior AP satisfies some auxiliary boundary condition at the inner boundary $r = R_0$. For example, in all the

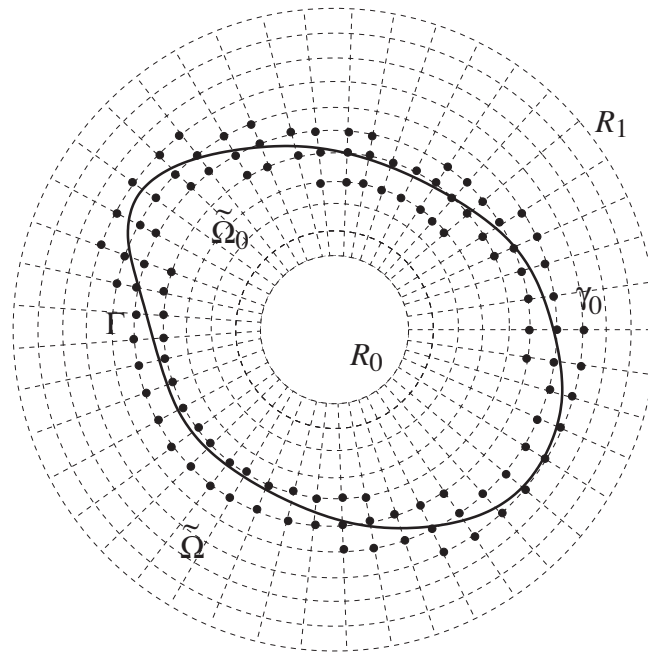


Fig. 3. Computational domain, grid, and the grid boundary γ_0 for the exterior subproblem.

computations of Section 3 we employ a homogeneous Dirichlet boundary condition at $r = R_0$. With these boundary conditions set at $r = R_0$ and $r = R_1$, the finite difference equation (31) is supposed to have a unique solution $u \in \mathfrak{U}_0$ for any g defined on the grid \mathbb{M}_0 . We denote this solution by $u = \mathbf{G}_0^{(h)} g$, where $\mathbf{G}_0^{(h)}$ is the Green’s operator of the discrete exterior AP, i.e., an inverse to $\mathbf{L}_0^{(h)}$ subject to $u \in \mathfrak{U}_0$.

The difference potential and boundary projection for the exterior subproblem are defined similarly to how it is done for the interior subproblem. Namely, the 9-point stencil of the operator $\mathbf{L}_0^{(h)}$ centered around a given node $m \equiv (i, j) \in \mathbb{M}_0$ is formally represented by the same expression (22). Then, similarly to (23a) we partition the nodes of \mathbb{M}_0 into two non-overlapping subsets:

$$\mathbb{M}_0^- = \mathbb{M}_0 \cap \tilde{\Omega} \quad \text{and} \quad \mathbb{M}_0^+ = \mathbb{M}_0 \cap \{\tilde{\Omega}_0 \setminus \tilde{\Omega}\} \tag{32a}$$

and define the subsets \mathbb{N}_0^- and \mathbb{N}_0^+ of the grid \mathbb{N}_0 by applying the stencil \mathbb{N}_m of (22) to each node of \mathbb{M}_0^- and \mathbb{M}_0^+ , respectively (cf. formula (23b)):

$$\mathbb{N}_0^- = \bigcup_{m \in \mathbb{M}_0^-} \mathbb{N}_m, \quad \mathbb{N}_0^+ = \bigcup_{m \in \mathbb{M}_0^+} \mathbb{N}_m. \tag{32b}$$

We emphasize that the notation in formulae (32a) and (32b) is the same as that in formulae (23a) and (23b), respectively, in the sense that the “-” nodes correspond to the exterior of Γ whereas the “+” nodes correspond to the interior of Γ .

The intersection of the sets \mathbb{N}_0^+ and \mathbb{N}_0^- of (32b) is called the exterior grid boundary:

$$\gamma_0 \stackrel{\text{def}}{=} \mathbb{N}_0^+ \cap \mathbb{N}_0^-. \tag{32c}$$

Similarly to the interior grid boundary γ_1 of (23c), the exterior grid boundary γ_0 of (32c) also looks like a multi-layer fringe of nodes near Γ , as shown schematically in Fig. 3.

Let ξ_{γ_0} be a grid function given on γ_0 and let $w \in \mathfrak{U}_0$ satisfy

$$\mathbf{T}_0^{(h)} w \stackrel{\text{def}}{=} w|_{\gamma_0} = \xi_{\gamma_0}$$

and be arbitrary otherwise. The exterior difference potential with the density ξ_{γ_0} is defined on the grid \mathbb{N}_0^- and given as follows (cf. formula (13))

$$\mathbf{P}_{\mathbb{N}_0^-} \xi_{\gamma_0} \stackrel{\text{def}}{=} w - \mathbf{G}_0^{(h)} \left(\chi_{\mathbb{M}_0^-} \mathbf{L}_0^{(h)} w \right). \tag{33}$$

In formula (33), $\chi_{\mathbb{M}_0^-} = 1$ on the grid \mathbb{M}_0^- and $\chi_{\mathbb{M}_0^-} = 0$ elsewhere on \mathbb{M}_0 . Similarly to the interior potential $\mathbf{P}_{\mathbb{N}_0^+} \xi_{\gamma_1}$ of (24), the exterior potential $\mathbf{P}_{\mathbb{N}_0^-} \xi_{\gamma_0}$ of (33) is insensitive to the choice of $w \in \mathfrak{U}_0$ as long as $\mathbf{T}_0^{(h)} w = \xi_{\gamma_0}$, and satisfies the homogeneous difference equation (cf. Eq. (25))

$$\mathbf{L}_0^{(h)} \left[\mathbf{P}_{\mathbb{N}_0^-} \xi_{\gamma_0} \right] = 0 \quad \text{on the grid } \mathbb{M}_0^-.$$

The discrete exterior boundary projection is defined as the trace of the potential (33) on the grid boundary γ_0 (cf. formula (9))

$$\mathbf{P}_{\gamma_0} \xi_{\gamma_0} \stackrel{\text{def}}{=} \mathbf{Tr}_0^{(h)} \mathbf{P}_{\mathbb{N}_0^-} \xi_{\gamma_0}. \tag{34}$$

A given $\xi_{\gamma_0}^{(\text{sc})}$ satisfies the discrete exterior BEP (cf. formula (15))

$$\mathbf{P}_{\gamma_0} \xi_{\gamma_0}^{(\text{sc})} = \xi_{\gamma_0}^{(\text{sc})} \tag{35}$$

if and only if there exists a function $u^{(\text{sc})}$ on the grid \mathbb{N}_0^- , called the scattering solution, that solves the difference equation (29) on the grid \mathbb{M}_0^- subject to the chosen ABC at $r = R_1$, and such that $\mathbf{Tr}_0^{(h)} u^{(\text{sc})} = \xi_{\gamma_0}^{(\text{sc})}$. If the BEP (35) holds, then the scattering solution $u^{(\text{sc})}$ is reconstructed on \mathbb{N}_0^- by means of the discrete generalized Green’s formula (cf. formula (16))

$$u^{(\text{sc})} = \mathbf{P}_{\mathbb{N}_0^-} \xi_{\gamma_0}^{(\text{sc})}. \tag{36}$$

The exterior BEP (35) is homogeneous, because there are no source terms that drive the scattering solution on $\tilde{\Omega}$. The overall exterior solution, however, is a superposition of the incident and scattered fields, see formula (30). A given ξ_{γ_0} is the trace of such a solution, $\xi_{\gamma_0} = \mathbf{Tr}_0^{(h)} u$, if and only if instead of (35) it satisfies the discrete exterior inhomogeneous BEP (cf. formula (17)):

$$\mathbf{P}_{\gamma_0} \xi_{\gamma_0} + (\mathbf{I}_{\gamma_0} - \mathbf{P}_{\gamma_0}) \xi_{\gamma_0}^{(\text{inc})} = \xi_{\gamma_0}, \tag{37}$$

where $\xi_{\gamma_0}^{(\text{inc})} = \mathbf{Tr}_0^{(h)} u^{(\text{inc})}$, and \mathbf{I}_{γ_0} is the identity operator in the space of grid functions defined on γ_0 . As in the continuous case (Section 1.3), if $u^{(\text{inc})}$ were generated by the sources on the grid \mathbb{M}^- , then we would have $\mathbf{P}_{\gamma_0} \xi_{\gamma_0}^{(\text{inc})} = 0$, and Eq. (37) would simplify to $\mathbf{P}_{\gamma_0} \xi_{\gamma_0} + \xi_{\gamma_0}^{(\text{inc})} = \xi_{\gamma_0}$.

If the BEP (37) holds, then solution (30) on the grid \mathbb{N}_0^- is given by (cf. formula (18))

$$u = \mathbf{P}_{\mathbb{N}_0^-} [\xi_{\gamma_0} - \xi_{\gamma_0}^{(\text{inc})}] + u^{(\text{inc})}. \tag{38}$$

Altogether, the discrete BEP (37) equivalently reduces the finite difference exterior subproblem, which consists of Eqs. (29), (30), and the ABC set at $r = R_1$ for $u^{(\text{sc})}$,³ from its grid domain \mathbb{N}_0^- to the grid boundary γ_0 . The solution of the BEP (37) on its own is not unique. However, when the exterior BEP (37) is coupled with the interior BEP (27), the resulting system of equations yields a unique solution to the overall transmission/scattering problem, see Section 2.3.

2.3. Matching at the interface

Hereafter, we assume that Γ is a smooth non-self intersecting plane closed curve, see Section 1.1. For a given two-component vector function $\xi_{\Gamma}^{(\Omega)} = (\xi_0, \xi_1)$, we introduce its extension from the curve Γ to the nodes of the interior grid boundary γ_1 , see formula (23c) and Fig. 2:

$$\xi_{\gamma_1} = \mathbf{E}\mathbf{x}_1 \xi_{\Gamma}^{(\Omega)}. \tag{39}$$

To construct the extension operator $\mathbf{E}\mathbf{x}_1$ of (39), we drop a normal from every node of γ_1 to the curve Γ , and use Taylor’s formula centered at the foot of this normal. In doing so, we interpret ξ_0 as the derivative of order zero, i.e., the function itself, and ξ_1 —as the derivative of order one in the direction normal to the curve Γ . To obtain higher order normal derivatives for the Taylor formula in (39), we use the differential equation (1a) and differentiate it several times. The details of this procedure are presented in [6]. Given that we use a fourth order accurate scheme for approximating Eq. (1a) on the grid, the highest order derivative that we need in the Taylor formula that defines the equation-based extension $\mathbf{E}\mathbf{x}_1$ is the fourth derivative. Hence, Eq. (1a) needs to be differentiated twice. This is convenient to do by first recasting this equation into the special orthogonal curvilinear coordinates associated with the curve Γ , see [6, Appendix A].

We emphasize that the equation-based extension (39) can be applied to any sufficiently smooth function $\xi_{\Gamma}^{(\Omega)}$. Its important property though is that if $\xi_{\Gamma}^{(\Omega)}$ happens to be the trace of a solution u to Eq. (1a) in the sense of (7), then there is convergence. Namely, let $u = u(\mathbf{x})$ be a solution to Eq. (1a) defined on the domain Ω' somewhat larger than $\Omega, \Omega \subset \Omega'$. This domain can coincide with the auxiliary domain Ω_1 introduced in Section 2.1, or it can be any other domain such that $\gamma_1 \subset \Omega'$. Then,

$$\|\mathbf{E}\mathbf{x}_1 \mathbf{Tr}_1 u - u|_{\gamma_1}\| = \mathcal{O}(h^5),$$

where the norm on the left-hand side is a discrete norm in the space of grid functions on γ_1 , and h is the size of the Cartesian discretization grid introduced in Section 2.1.

Similarly, for a given two-component vector function $\xi_{\Gamma}^{(\tilde{\Omega})}$ we introduce its equation-based extension from the curve Γ to the exterior grid boundary γ_0 , see formula (32c) and Fig. 3:

³ The continuous exterior subproblem consists of Eqs. (1b), (4) on $\tilde{\Omega}$ and the radiation condition (5) at infinity.

$$\xi_{\gamma_0} = \mathbf{E}\mathbf{x}_0\xi_{\Gamma}^{(\Omega)}. \tag{40}$$

Extension (40) employs the Taylor formula with the derivatives up to order four obtained by differentiating the differential equation (1b). If $u = u(\mathbf{x})$ is a solution to Eq. (1b) defined on a region $\tilde{\Omega}' \supset \gamma_0$, then

$$\|\mathbf{E}\mathbf{x}_0\mathbf{Tr}_0u - u|_{\gamma_0}\| = \mathcal{O}(h^5),$$

where the norm on the left-hand side is a discrete norm in the space of grid functions on γ_0 , and h is the size of the polar discretization grid introduced in Section 2.2.

Next, we introduce a basis in the space of functions $\xi_{\Gamma}^{(\Omega)}$ and in the space of functions $\xi_{\Gamma}^{(\tilde{\Omega})}$. It does not have to be the same basis, but choosing it the same simplifies the analysis with no loss of generality. As both $\xi_{\Gamma}^{(\Omega)}$ and $\xi_{\Gamma}^{(\tilde{\Omega})}$ are vector functions with two components, the basis functions are taken in the form

$$\psi_j^{(0)} \equiv (\psi_j, 0) \quad \text{and} \quad \psi_j^{(1)} \equiv (0, \psi_j), \quad j = 0, \pm 1, \pm 2, \dots, \tag{41}$$

where ψ_j are conventional scalar functions on the curve Γ . For example, we can choose

$$\psi_j(s) = e^{ij\frac{2\pi}{S}s}, \tag{42}$$

where $0 \leq s \leq S$ is the arc length along Γ . In this case, the expansion of a given (ξ_0, ξ_1) with respect to the basis (41) becomes a Fourier series for each of the two components:

$$\begin{aligned} \xi_0(s) &= \sum_{j=-\infty}^{\infty} c_j^{(0)} e^{ij\frac{2\pi}{S}s}, \quad \text{where } c_j^{(0)} = \frac{1}{S} \int_0^S \xi_0(s) e^{-ij\frac{2\pi}{S}s} ds, \\ \xi_1(s) &= \sum_{j=-\infty}^{\infty} c_j^{(1)} e^{ij\frac{2\pi}{S}s}, \quad \text{where } c_j^{(1)} = \frac{1}{S} \int_0^S \xi_1(s) e^{-ij\frac{2\pi}{S}s} ds. \end{aligned}$$

Since for a smooth function $\xi_0(s)$ or $\xi_1(s)$ its Fourier series converges rapidly, in practice we can truncate the expansions:

$$\xi_0(s) \approx \sum_{j=-M}^M c_j^{(0)} \psi_j(s) \quad \text{and} \quad \xi_1(s) \approx \sum_{j=-M}^M c_j^{(1)} \psi_j(s), \tag{43}$$

where M is to be chosen ahead of time so as to guarantee that the accuracy of representation (43) will exceed any accuracy that can be attained on the grid. It is the coefficients $c_j^{(0)}$ and $c_j^{(1)}$, $j = -M, \dots, M$, in formulae (43) that will be the unknowns to be determined when solving the combined system of the interior and exterior BEP, (27) and (37).

Specifically, we look for the interior trace $\xi_{\Gamma}^{(\Omega)}$ in the form of a finite sum

$$\xi_{\Gamma}^{(\Omega)} = \sum_{j=-M}^M [c_j^{(0,\Omega)} \psi_j^{(0)} + c_j^{(1,\Omega)} \psi_j^{(1)}] \tag{44}$$

with the undetermined coefficients $c_j^{(0,\Omega)}$ and $c_j^{(1,\Omega)}$, $j = -M, \dots, M$. Applying the equation-based extension $\mathbf{E}\mathbf{x}_1$ of (39) to the expression (44), we have:

$$\xi_{\gamma_1} = \sum_{j=-M}^M [c_j^{(0,\Omega)} \mathbf{E}\mathbf{x}_1 \psi_j^{(0)} + c_j^{(1,\Omega)} \mathbf{E}\mathbf{x}_1 \psi_j^{(1)}],$$

and substituting this ξ_{γ_1} into the interior BEP (27), we arrive at the following system of linear algebraic equations for the unknowns $c_j^{(0,\Omega)}$ and $c_j^{(1,\Omega)}$, $j = -M, \dots, M$:

$$\sum_{j=-M}^M [c_j^{(0,\Omega)} (\mathbf{P}_{\gamma_1} - \mathbf{I}_{\gamma_1}) \mathbf{E}\mathbf{x}_1 \psi_j^{(0)} + c_j^{(1,\Omega)} (\mathbf{P}_{\gamma_1} - \mathbf{I}_{\gamma_1}) \mathbf{E}\mathbf{x}_1 \psi_j^{(1)}] = -\mathbf{Tr}_1^{(h)} \mathbf{G}_1^{(h)} \mathbf{B}_1^{(h)} \bar{\mathbf{f}}, \tag{45}$$

where \mathbf{I}_{γ_1} is the identity operator in the space of grid functions defined on the grid boundary γ_1 . System (45) can be recast in the matrix form:

$$\mathbf{Q}_{\gamma_1} \mathbf{c}^{(\Omega)} = -\mathbf{Tr}_1^{(h)} \mathbf{G}_1^{(h)} \mathbf{B}_1^{(h)} \bar{\mathbf{f}}, \tag{46}$$

where $\mathbf{c}^{(\Omega)} = [c_{-M}^{(0,\Omega)}, \dots, c_M^{(0,\Omega)}, c_{-M}^{(1,\Omega)}, \dots, c_M^{(1,\Omega)}]^T$ is the vector of unknowns, and \mathbf{Q}_{γ_1} is a matrix of $2(2M + 1)$ columns obtained by applying the composition of operators $(\mathbf{P}_{\gamma_1} - \mathbf{I}_{\gamma_1}) \mathbf{E}\mathbf{x}_1$ to the individual basis functions $\psi_j^{(0)}$ and $\psi_j^{(1)}$ of (41). The vertical dimension of the matrix \mathbf{Q}_{γ_1} of (46) is equal to $|\gamma_1|$, where the grid boundary γ_1 consists of $|\gamma_1|$ grid nodes.

Similarly, we express the exterior trace $\xi_{\Gamma}^{(\tilde{\Omega})}$ in the form of a finite sum

$$\xi_{\Gamma}^{(\tilde{\Omega})} = \sum_{j=-M}^M [c_j^{(0,\tilde{\Omega})} \psi_j^{(0)} + c_j^{(1,\tilde{\Omega})} \psi_j^{(1)}], \tag{47}$$

where the coefficients $c_j^{(0,\tilde{\Omega})}$ and $c_j^{(1,\tilde{\Omega})}$, $j = -M, \dots, M$, are also to be determined. Applying the equation-based extension $\mathbf{E}\mathbf{x}_0$ of (40) to the expression (47), we have:

$$\xi_{\gamma_0} = \sum_{j=-M}^M [c_j^{(0,\tilde{\Omega})} \mathbf{E}\mathbf{x}_0 \psi_j^{(0)} + c_j^{(1,\tilde{\Omega})} \mathbf{E}\mathbf{x}_0 \psi_j^{(1)}]$$

and substituting this ξ_{γ_0} into the interior BEP (37), we arrive at the following system of linear algebraic equations with respect to the unknowns $c_j^{(0,\tilde{\Omega})}$ and $c_j^{(1,\tilde{\Omega})}$, $j = -M, \dots, M$:

$$\sum_{j=-M}^M [c_j^{(0,\tilde{\Omega})} (\mathbf{P}_{\gamma_0} - \mathbf{I}_{\gamma_0}) \mathbf{E}\mathbf{x}_0 \psi_j^{(0)} + c_j^{(1,\tilde{\Omega})} (\mathbf{P}_{\gamma_0} - \mathbf{I}_{\gamma_0}) \mathbf{E}\mathbf{x}_0 \psi_j^{(1)}] = (\mathbf{P}_{\gamma_0} - \mathbf{I}_{\gamma_0}) \xi_{\gamma_0}^{(\text{inc})}. \tag{48}$$

System (48) can be recast in the matrix form:

$$\mathbf{Q}_{\gamma_0} \mathbf{c}^{(\tilde{\Omega})} = (\mathbf{P}_{\gamma_0} - \mathbf{I}_{\gamma_0}) \xi_{\gamma_0}^{(\text{inc})}, \tag{49}$$

where $\mathbf{c}^{(\tilde{\Omega})} = [c_{-M}^{(0,\tilde{\Omega})}, \dots, c_M^{(0,\tilde{\Omega})}, c_{-M}^{(1,\tilde{\Omega})}, \dots, c_M^{(1,\tilde{\Omega})}]^T$ is the vector of unknowns, and \mathbf{Q}_{γ_0} is a matrix of $2(2M + 1)$ columns obtained by applying the composition of operators $(\mathbf{P}_{\gamma_0} - \mathbf{I}_{\gamma_0}) \mathbf{E}\mathbf{x}_0$ to the individual basis functions $\psi_j^{(0)}$ and $\psi_j^{(1)}$ of (41). The vertical dimension of the matrix \mathbf{Q}_{γ_0} of (49) is equal to $|\gamma_0|$, where the grid boundary γ_0 consists of $|\gamma_0|$ grid nodes.

The resulting two systems (46) and (49) are solved as one large coupled system with respect to the combined unknowns $\mathbf{c}^{(\tilde{\Omega})}$ and $\mathbf{c}^{(\tilde{\Omega})}$. In doing so, the interface conditions discussed in Section 1.1 provides additional relations between the coefficients $\mathbf{c}^{(\tilde{\Omega})}$ and $\mathbf{c}^{(\tilde{\Omega})}$. The simplest interface condition (6) or, equivalently, (19), implies that $\mathbf{c}^{(\tilde{\Omega})} = \mathbf{c}^{(\tilde{\Omega})}$. Then, denoting the common vector of unknowns by $\mathbf{c} = [c_{-M}^{(0)}, \dots, c_M^{(0)}, c_{-M}^{(1)}, \dots, c_M^{(1)}]^T$, we obtain the following coupled system based on (46), (49):

$$\begin{cases} \mathbf{Q}_{\gamma_1} \mathbf{c} = -\mathbf{T}\mathbf{r}_1^{(h)} \mathbf{G}_1^{(h)} \mathbf{B}_1^{(h)} \bar{\mathbf{f}}, \\ \mathbf{Q}_{\gamma_0} \mathbf{c} = (\mathbf{P}_{\gamma_0} - \mathbf{I}_{\gamma_0}) \xi_{\gamma_0}^{(\text{inc})}. \end{cases} \tag{50}$$

System (50) which has dimension $2(2M + 1) \times (|\gamma_1| + |\gamma_0|)$ is to be solved in the sense of the least squares, i.e., by a QR decomposition. Once the vector of coefficients \mathbf{c} has been determined, it is substituted into both (44) and (47) to obtain $\xi_{\Gamma}^{(\tilde{\Omega})}$ and $\xi_{\Gamma}^{(\tilde{\Omega})}$, respectively. Then, the discrete traces ξ_{γ_1} and ξ_{γ_0} are obtained by applying the corresponding extension operators:

$$\xi_{\gamma_1} = \mathbf{E}\mathbf{x}_1 \xi_{\Gamma}^{(\tilde{\Omega})} \quad \text{and} \quad \xi_{\gamma_0} = \mathbf{E}\mathbf{x}_0 \xi_{\Gamma}^{(\tilde{\Omega})}$$

and finally, the interior and exterior parts of the overall solution are evaluated on the grids \mathbb{N}_1^+ and \mathbb{N}_0^- by means of the discrete Green's formulae (28) and (38), respectively.

The rate of the grid convergence of the numerical algorithm that we have described coincides with the design accuracy of its constituent schemes (21) and (29). As both schemes we have chosen, [18] and [17], are fourth order accurate, the combined methodology based on difference potentials also yields fourth order convergence. This is corroborated by a series of numerical experiments presented in Section 3. For the theoretical convergence analysis of the method of difference potentials, we refer the reader to the work by Reznik [21], a brief account of which can be found in our recent paper [6], as well as to the monograph [5], which offers a considerably more detailed discussion. The analysis of the well-posedness of the resulting boundary formulation that appears in the context of the method of difference potentials can also be found in [5].

2.4. Pure scattering problems

Assume we wish to solve a pure exterior scattering problem, for which there is no refraction at the interface Γ and no transmission of waves from $\tilde{\Omega}$ to Ω , see Fig. 1. Instead, the incident waves get scattered off (i.e., reflected from) a given shape Ω , subject to a boundary condition specified at Γ . In this case, the foregoing numerical algorithm is simplified.

Consider the constant coefficient homogeneous Helmholtz equation (1b) on the exterior domain $\tilde{\Omega}$, see Fig. 1, subject to either a Dirichlet boundary condition or a Neumann boundary condition at the boundary Γ . The boundary condition is set for the total field:

$$u|_{\Gamma} = 0 \tag{51a}$$

or

$$\left. \frac{\partial u}{\partial \mathbf{n}} \right|_{\Gamma} = 0. \tag{51b}$$

Taking into account expression (4), boundary conditions ((51)) can be equivalently recast as

$$u^{(\text{sc})}|_{\Gamma} = -u^{(\text{inc})}|_{\Gamma} \equiv \phi_0(s) \tag{52a}$$

or

$$\frac{\partial \mathbf{u}^{(\text{sc})}}{\partial \mathbf{n}} \Big|_{\Gamma} = - \frac{\partial \mathbf{u}^{(\text{inc})}}{\partial \mathbf{n}} \Big|_{\Gamma} \equiv \phi_1(s), \tag{52b}$$

where the functions $\phi_0(s)$ and $\phi_1(s)$ are given on the curve Γ . Hence, the entire exterior problem can be solved with respect to the scattered field $\mathbf{u}^{(\text{sc})} = \mathbf{u}^{(\text{sc})}(\mathbf{x})$ only. If the field u is interpreted as acoustic pressure, then the Dirichlet boundary condition (52a) corresponds to sound-soft scattering, and the Neumann boundary condition (52b) corresponds to sound-hard scattering.

Since, we are solving for the scattered field, we need to employ the homogeneous exterior BEP (35) and, accordingly, a homogeneous counterpart of system (49):

$$\mathbf{Q}_{\gamma_0} \mathbf{c} = \mathbf{0}. \tag{53}$$

The vector of unknowns \mathbf{c} in system (53) consists of two sub-vectors: $\mathbf{c} = [\mathbf{c}^{(0)}, \mathbf{c}^{(1)}]$, where $\mathbf{c}^{(0)} = [c_{-M}^{(0)}, \dots, c_M^{(0)}]^T$ are the expansion coefficients of the Dirichlet data of the solution at the boundary Γ with respect to the basis functions (42), and $\mathbf{c}^{(1)} = [c_{-M}^{(1)}, \dots, c_M^{(1)}]^T$ are the expansion coefficients of the Neumann data of the solution at the boundary Γ .

For a Dirichlet boundary condition specified at Γ , see (52a), the Dirichlet data $\phi_0(s)$ are given, and hence the coefficients $\mathbf{c}^{(0)} = [c_{-M}^{(0)}, \dots, c_M^{(0)}]^T$ are considered known:

$$c_j^{(0)} = \frac{1}{S} \int_0^S \phi_0(s) e^{-ij\frac{2\pi}{S}s} ds, \quad j = -M, \dots, M.$$

Then, the Neumann coefficients $\mathbf{c}^{(1)} = [c_{-M}^{(1)}, \dots, c_M^{(1)}]^T$ are determined from system (53), which takes the form:

$$\mathbf{Q}_{\gamma_0}^{(1)} \mathbf{c}^{(1)} = \underbrace{-\mathbf{Q}_{\gamma_0}^{(0)} \mathbf{c}^{(0)}}_{\text{given data}}. \tag{54a}$$

For a Neumann boundary condition specified at Γ , see (52b), the Neumann data $\phi_1(s)$ are given, and hence the coefficients $\mathbf{c}^{(1)} = [c_{-M}^{(1)}, \dots, c_M^{(1)}]^T$ are considered known:

$$c_j^{(1)} = \frac{1}{S} \int_0^S \phi_1(s) e^{-ij\frac{2\pi}{S}s} ds, \quad j = -M, \dots, M.$$

Then, the Dirichlet coefficients $\mathbf{c}^{(0)} = [c_{-M}^{(0)}, \dots, c_M^{(0)}]^T$ are determined by solving the system derived from (53):

$$\mathbf{Q}_{\gamma_0}^{(0)} \mathbf{c}^{(0)} = \underbrace{-\mathbf{Q}_{\gamma_0}^{(1)} \mathbf{c}^{(1)}}_{\text{given data}}. \tag{54b}$$

The partition of the matrix \mathbf{Q}_{γ_0} into $\mathbf{Q}_{\gamma_0}^{(0)}$ and $\mathbf{Q}_{\gamma_0}^{(1)}$ in formulae ((54)) is done in accordance with the partition of the vector of unknowns \mathbf{c} into $\mathbf{c}^{(0)}$ and $\mathbf{c}^{(1)}$. Each of the systems (54a) or (54b) is solved in the sense of least squares by means of the QR decomposition. Once the entire vector of coefficients $\mathbf{c} = [\mathbf{c}^{(0)}, \mathbf{c}^{(1)}]$ is obtained, it is substituted into formula (47), which yields $\xi_{\Gamma}^{(\Omega)}$. The latter, in turn, is extended from the continuous boundary Γ to the grid boundary γ_0 with the help of the operator (40), and finally, the exterior solution on the grid \mathbb{N}_0^- is determined by means of the discrete Green's formula (36).

3. Numerical simulations

In this section, we present computational results for two types of formulations—pure exterior scattering problems and transmission/scattering problems.

3.1. Exterior scattering problems

We consider the scattering of an incoming plane wave with a given frequency (wavelength) and given angle of incidence about an elliptical shape with a given aspect ratio. In our simulations, we take the major semi-axis of the ellipse to be $a = 1.8$, while its minor semi-axis varies between $b = 0.9$ and $b = 0.18$, which yields aspect ratios between 2 and 10. The wavenumber in the Helmholtz equation (1b) varies between $k_0 = 1$ and $k_0 = 25$, which yields the variation of the wavelength between $\lambda_0 = 2\pi$ and $\lambda_0 = 2\pi/25$, i.e., between roughly twice the size $2a$ of the ellipse and about 8% of this size. We consider several values of the angle of incidence between 0° and 50° with respect to the direction of the major axis. We also consider both Dirichlet and Neumann boundary conditions at the contour Γ , i.e., at the perimeter of the ellipse. In the context of acoustics, the former corresponds to sound-soft scattering, whereas the latter corresponds to sound-hard scattering. The exterior AP is solved on the domain $\tilde{\Omega}_0$ shaped as an annulus, $\tilde{\Omega}_0 = \{R_0 \leq r \leq R_1\}$, see Fig. 3, with R_0 that may vary between 0.1 (for larger aspect ratios) and 0.3 (for smaller aspect ratios), and $R_1 = 2$. This AP is discretized on a uniform in each direction polar grid that may have between 128×128 and 4096×4096 cells. The quantity M that represents the dimension of the basis on Γ , see formula (43), is grid-independent and chosen so as to guarantee that the given boundary data (Dirichlet or Neumann) are approximated by the corresponding finite Fourier series up to the machine precision. This yields a very conservative estimate

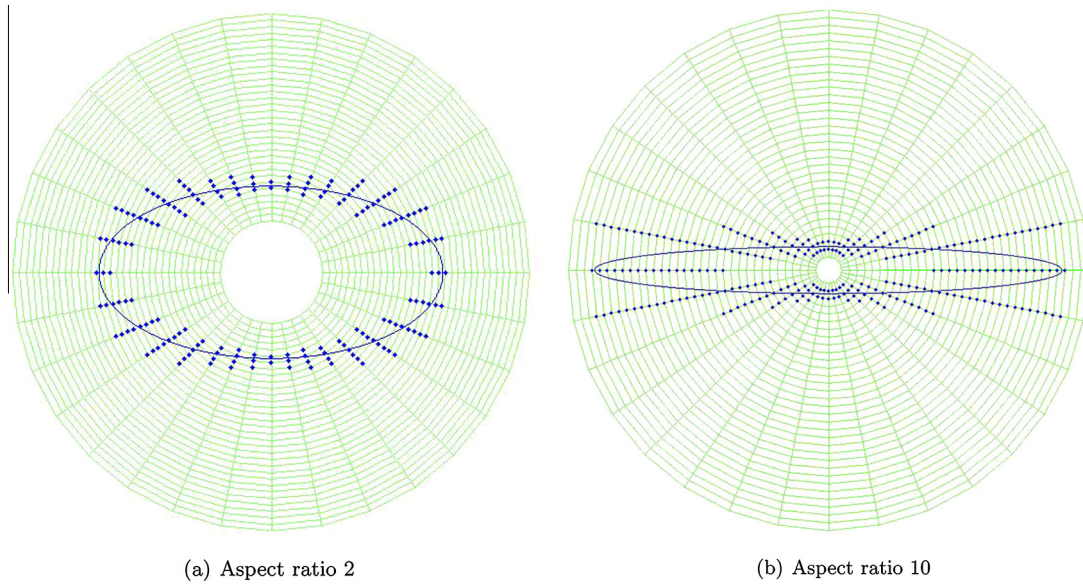


Fig. 4. Schematic of the polar grid for the exterior AP, the elliptic scatterer, and the grid boundary γ .

for M . For better efficiency, one would choose M large enough so that truncating the series gives an error much smaller than the discretization error, which implies that M would be grid-dependent. The problem is solved using the simplified methodology of Section 2.4. In doing so, the discrete exterior AP is integrated by means of the separation of variables combined with FFT. The exact nonlocal ABC at the outer circle $r = R_1$, Fig. 3, is then formulated in Fourier space, see [17].

As the overall set of results for all wavenumbers, incidence angles, aspect ratios, etc., is rather large, we have chosen to show only a representative sample. In Fig. 4, we show the schematic geometry for two ellipses—of aspect ratio 2 and of aspect ratio 10 (cf. Fig. 3).

To assess the grid convergence, we do not evaluate the exact solution using its expansion with respect to Mathieu functions [22], because this may entail numerical difficulties in evaluating high order Mathieu functions. Instead, we evaluate the maximum norm (over the entire solution domain) of the difference between the numerical solutions obtained on two consecutive grids, $u^{(h)}$ and $u^{(2h)}$.

Tables 1–3 demonstrate the design fourth order rate of grid convergence for the case of a Dirichlet boundary condition on Γ . We note that the convergence on coarser grids looks somewhat more “erratic” for slenderer ellipses. This is likely accounted for by insufficient grid resolution in the areas of high curvature, i.e., near the tips of the major axis. Nonetheless, on finer grids the convergence rate approaches its correct asymptotic value of 4. Similar results are obtained for the Neumann boundary condition on Γ , see Tables 4 and 5, as well as for a variety of other Dirichlet and Neumann cases that are not presented in these tables.

We emphasize that the scheme converges with the same design rate for all angles of incidence, all wavenumbers, and all aspect ratios. The actual values of the error may depend on the specific parameters involved. For example, from Tables 1–5 one can see that as the wavenumber k_0 increases while all other parameters remain the same (the aspect ratio, the grid, etc.), the maximum norm error (evaluated across the domain) also increases. On the other hand, the angle of incidence does not affect the convergence rate and does not noticeably affect the error. In Fig. 5, we show the dependence of the error on the angle of incidence for both sound-soft (Dirichlet boundary condition) and sound-hard (Neumann boundary condition) scattering about an ellipse of aspect ratio 3. We see that for both $k_0 = 3$ and $k_0 = 30$ the error changes by a factor of less than 2 over the entire 90° span.

Table 1
Sound-soft scattering of a plane wave with incidence angle 35° about an ellipse with aspect ratio 2.

Grid	$k_0 = 1, M = 12$		$k_0 = 10, M = 37$		$k_0 = 25, M = 69$	
	$\ u^{(h)} - u^{(2h)}\ _\infty$	Conv. rate	$\ u^{(h)} - u^{(2h)}\ _\infty$	Conv. rate	$\ u^{(h)} - u^{(2h)}\ _\infty$	Conv. rate
128×128	3.686772×10^{-4}	–	9.024242×10^{-2}	–	2.571935×10^1	–
256×256	2.092322×10^{-5}	4.1392	5.042251×10^{-3}	4.1617	4.528627×10^{-1}	5.8276
512×512	1.140182×10^{-6}	4.1978	3.077507×10^{-4}	4.0342	2.614107×10^{-2}	4.1147
1024×1024	7.045679×10^{-8}	4.0164	1.912254×10^{-5}	4.0084	1.576210×10^{-3}	4.0518
2048×2048	4.352290×10^{-9}	4.0169	1.193405×10^{-6}	4.0021	9.766250×10^{-5}	4.0125
4096×4096	2.708936×10^{-10}	4.0060	7.456103×10^{-8}	4.0005	6.090803×10^{-6}	4.0031

Table 2Sound-soft scattering of a plane wave with incidence angle 15° about an ellipse with aspect ratio 5.

Grid	$k_0 = 1, M = 13$		$k_0 = 10, M = 39$		$k_0 = 25, M = 73$	
	$\ u^{(h)} - u^{(2h)}\ _\infty$	Conv. rate	$\ u^{(h)} - u^{(2h)}\ _\infty$	Conv. rate	$\ u^{(h)} - u^{(2h)}\ _\infty$	Conv. rate
128×128	1.117795×10^1	–	1.080259×10^1	–	2.905446×10^3	–
256×256	8.069814×10^{-3}	10.4358	5.008329×10^{-2}	7.7528	6.346536×10^{-1}	12.1605
512×512	1.523137×10^{-3}	2.4055	5.161442×10^{-3}	3.2785	2.456628×10^{-2}	4.6912
1024×1024	7.604331×10^{-5}	4.3241	4.003719×10^{-4}	3.6884	1.471074×10^{-3}	4.0617
2048×2048	3.763327×10^{-6}	4.3367	1.942630×10^{-5}	4.3653	9.124847×10^{-5}	4.0109
4096×4096	2.072289×10^{-7}	4.1827	1.066348×10^{-6}	4.1873	5.691707×10^{-6}	4.0029

Table 3Sound-soft scattering of a plane wave with incidence angle 50° about an ellipse with aspect ratio 10.

Grid	$k_0 = 1, M = 11$		$k_0 = 10, M = 32$		$k_0 = 25, M = 56$	
	$\ u^{(h)} - u^{(2h)}\ _\infty$	Conv. rate	$\ u^{(h)} - u^{(2h)}\ _\infty$	Conv. rate	$\ u^{(h)} - u^{(2h)}\ _\infty$	Conv. rate
128×128	5.212738×10^2	–	4.701542×10^2	–	1.547453×10^5	–
256×256	8.031341×10^2	–0.6236	4.419326×10^2	0.0893	8.284062×10^3	7.5453
512×512	1.195681×10^{-2}	16.0355	4.052018×10^{-1}	10.0910	9.340049×10^{-1}	9.7927
1024×1024	4.655482×10^{-3}	1.3608	2.785232×10^{-2}	3.8628	8.518332×10^{-2}	3.4548
2048×2048	5.918121×10^{-4}	2.9757	1.895585×10^{-3}	3.8771	2.569198×10^{-3}	5.0512
4096×4096	2.142775×10^{-5}	4.7876	8.621134×10^{-5}	4.4586	1.937799×10^{-4}	3.7288

Table 4Sound-hard scattering of a plane wave with incidence angle 0° about an ellipse with aspect ratio 3.

Grid	$k_0 = 1, M = 14$		$k_0 = 10, M = 43$		$k_0 = 25, M = 79$	
	$\ u^{(h)} - u^{(2h)}\ _\infty$	Conv. rate	$\ u^{(h)} - u^{(2h)}\ _\infty$	Conv. rate	$\ u^{(h)} - u^{(2h)}\ _\infty$	Conv. rate
128×128	9.846534×10^{-3}	–	1.448027×10^{-1}	–	4.461393×10^1	–
256×256	1.884702×10^{-4}	5.7072	8.659281×10^{-3}	4.0637	5.844125×10^{-1}	6.2544
512×512	9.615561×10^{-6}	4.2928	2.363689×10^{-4}	5.1951	2.368270×10^{-2}	4.6251
1024×1024	4.412894×10^{-7}	4.4456	1.470104×10^{-5}	4.0071	1.454638×10^{-3}	4.0251
2048×2048	2.845780×10^{-8}	3.9548	9.188393×10^{-7}	4.0000	9.027833×10^{-5}	4.0101
4096×4096	1.589844×10^{-9}	4.1619	5.934903×10^{-8}	3.9525	5.631228×10^{-6}	4.0029

Table 5Sound-hard scattering of a plane wave with incidence angle 50° about an ellipse with aspect ratio 5.

Grid	$k_0 = 1, M = 13$		$k_0 = 10, M = 35$		$k_0 = 25, M = 61$	
	$\ u^{(h)} - u^{(2h)}\ _\infty$	Conv. rate	$\ u^{(h)} - u^{(2h)}\ _\infty$	Conv. rate	$\ u^{(h)} - u^{(2h)}\ _\infty$	Conv. rate
128×128	1.076195	–	1.602327	–	6.882858×10^1	–
256×256	1.593996×10^{-1}	2.7552	5.157602×10^{-1}	1.6354	2.620046	4.7153
512×512	1.921666×10^{-3}	6.3741	9.974005×10^{-3}	5.6924	3.826752×10^{-2}	6.0973
1024×1024	3.456720×10^{-5}	5.7968	2.426475×10^{-4}	5.3612	1.628882×10^{-3}	4.5542
2048×2048	3.522082×10^{-6}	3.2949	1.769029×10^{-5}	3.7778	1.062220×10^{-4}	3.9387
4096×4096	1.822888×10^{-7}	4.2721	9.543673×10^{-7}	4.2123	6.264534×10^{-6}	4.0837

A clear advantage of our method is that scattering off a given shape but for multiple angles of incidence, and even for different boundary conditions, can be computed very efficiently. This is particularly important if the direct scattering problem needs to be solved many times while using an iterative method to solve an inverse scattering problem.

For a given basis on Γ , see formulae (41), (42), and a given discretization grid, the matrix \mathbf{Q}_{γ_0} that is introduced by formulae (48), (49) and then used in equation (53) needs to be computed only once. Each new angle of incidence only requires choosing a new vector of known coefficients $\mathbf{c}^{(0)}$ in formula (54a) in the case of sound-soft scattering or a new vector of known coefficients $\mathbf{c}^{(1)}$ in formula (54b) in the case of sound-hard scattering. The corresponding costs are obviously negligible. Other, more elaborate, types of scattering (i.e., boundary conditions) can also be accommodated using the same matrix

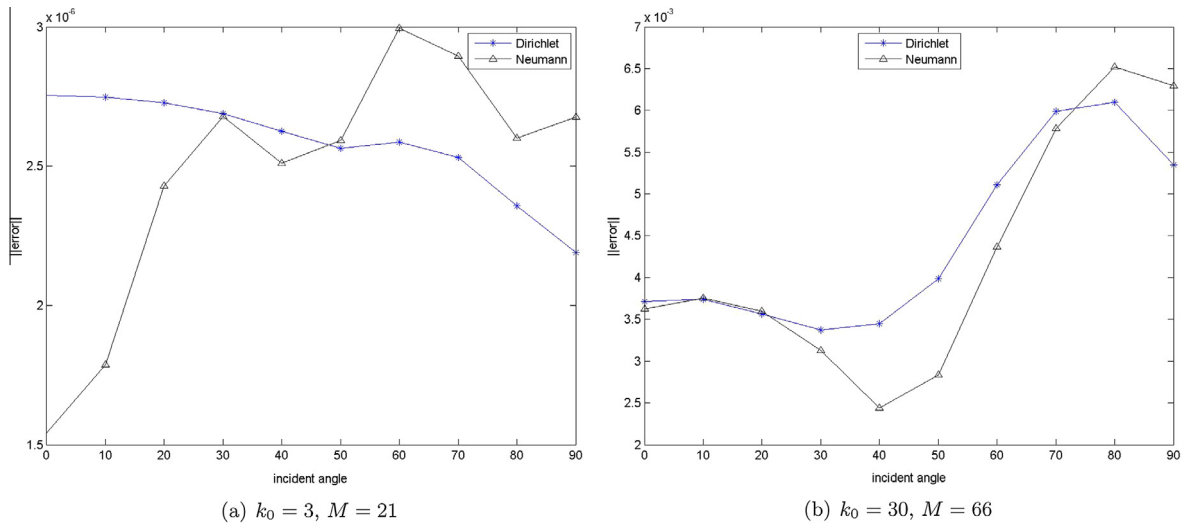


Fig. 5. Error vs. the angle of incidence for sound-soft (Dirichlet BC) and sound-hard (Neumann BC) scattering about an ellipse with aspect ratio 3 computed on the polar grid of dimension 1024×1024 .

\mathbf{Q}_{γ_0} , see [23]. Both systems ((54)) are solved by a QR decomposition. Each of the matrices $\mathbf{Q}_{\gamma_0}^{(1)}$ and $\mathbf{Q}_{\gamma_0}^{(0)}$ needs to be decomposed only once, and then solutions for multiple angles of incidence and a given type of scattering can be computed by backward substitution. In practice though, the cost of a QR decomposition was also found to be negligible. Finally, once the full vector of coefficients $\mathbf{c} = [\mathbf{c}^{(0)}, \mathbf{c}^{(1)}]$ has been determined, $\xi_{\Gamma}^{(\Omega)}$ is obtained by formula (47), then extended from Γ to γ_0 using (40), and the exterior solution on \mathbb{N}_0 is computed with the help of formula (36). The latter is the only non-negligible computational expense per angle of incidence.

For our MATLAB implementation, the one-time computation of the matrix \mathbf{Q}_{γ_0} for all the cases presented in Fig. 5(a) (a 1024×1024 grid) took approximately 36 s, whereas the subsequent computation of the 20 Dirichlet and Neumann scattering solutions (10° increments in the angle of incidence between 0° and 90° for either boundary condition) took only 0.8 s each. Similarly, the one-time computation of the matrix \mathbf{Q}_{γ_0} for all the cases presented in Fig. 5(b) required about 91 s. Subsequently, it took only about 0.7 s per angle of incidence for either the sound-soft or sound-hard scattering.

3.2. Transmission/scattering problems with piecewise constant coefficients

The numerical simulation of the transmission and scattering of waves about a given shape (an ellipse) is done using the computational framework similar to that of Section 3.1, except that instead of setting a boundary condition on Γ we assume

Table 6
Transmission and scattering of a plane wave with incidence angle 40° about an ellipse with aspect ratio 3.

	$M = 18$ Exterior, $k_0 = 1$		$M = 43$ Exterior, $k_0 = 5$		$M = 70$ Exterior, $k_0 = 10$		
	$\ u^{(h)} - u^{(2h)}\ _\infty$	Conv. rate	$\ u^{(h)} - u^{(2h)}\ _\infty$	Conv. rate	$\ u^{(h)} - u^{(2h)}\ _\infty$	Conv. rate	
<i>Ext. grid</i>							
128 × 128	5.257675×10^{-4}	–	1.222531	–	2.540071	–	
256 × 256	2.968034×10^{-5}	4.1468	1.256795×10^{-2}	6.6040	2.505713	0.0196	
512 × 512	1.621693×10^{-6}	4.1939	7.215245×10^{-4}	4.1226	5.294069×10^{-2}	5.5647	
1024 × 1024	8.319173×10^{-8}	4.2849	4.686281×10^{-5}	3.9445	3.040675×10^{-3}	4.1219	
2048 × 2048	5.185747×10^{-9}	4.0038	2.980399×10^{-6}	3.9749	1.824703×10^{-4}	4.0587	
<i>Int. grid</i>							
		$M = 18$ Interior, $k_1 = 3$		$M = 43$ Interior, $k_1 = 15$		$M = 70$ Interior, $k_1 = 30$	
		$\ u^{(h)} - u^{(2h)}\ _\infty$	Conv. rate	$\ u^{(h)} - u^{(2h)}\ _\infty$	Conv. rate	$\ u^{(h)} - u^{(2h)}\ _\infty$	Conv. rate
128 × 128	4.727249×10^{-4}	–	1.476710	–	1.454990×10^1	–	
256 × 256	9.910096×10^{-6}	5.5760	7.240317×10^{-2}	4.3502	3.219025	2.1763	
512 × 512	8.298524×10^{-7}	3.5780	7.604703×10^{-4}	6.5730	5.533717×10^{-2}	5.8622	
1024 × 1024	3.405935×10^{-8}	4.6067	5.105078×10^{-5}	3.8969	3.352915×10^{-3}	4.0448	
2048 × 2048	2.025545×10^{-9}	4.0717	3.330358×10^{-6}	3.9382	2.093157×10^{-4}	4.0017	

Table 7Transmission and scattering of a plane wave with incidence angle 40° about an ellipse with aspect ratio 12.

	$M = 17$ Exterior, $k_0 = 1$		$M = 42$ Exterior, $k_0 = 5$		$M = 68$ Exterior, $k_0 = 10$	
	$\ u^{(h)} - u^{(2h)}\ _\infty$	Conv. rate	$\ u^{(h)} - u^{(2h)}\ _\infty$	Conv. rate	$\ u^{(h)} - u^{(2h)}\ _\infty$	Conv. rate
<i>Ext. grid</i>						
128 × 128	3.339419	–	1.011317×10^2	–	8.966609×10^2	–
256 × 256	2.525248×10^{-3}	10.3690	4.429088	4.5131	1.265494×10^1	6.1468
512 × 512	3.016655×10^{-4}	3.0654	3.727909×10^{-2}	6.8925	5.603543×10^{-1}	4.4972
1024 × 1024	7.296313×10^{-5}	2.0477	4.070004×10^{-3}	3.1953	6.315946×10^{-3}	6.4712
2048 × 2048	9.046537×10^{-6}	3.0117	3.237602×10^{-4}	3.6520	3.668013×10^{-4}	4.1059
<i>Int. grid</i>						
	$k_1 = 3$		$k_1 = 15$		$k_1 = 30$	
	$\ u^{(h)} - u^{(2h)}\ _\infty$	Conv. rate	$\ u^{(h)} - u^{(2h)}\ _\infty$	Conv. rate	$\ u^{(h)} - u^{(2h)}\ _\infty$	Conv. rate
128 × 128	2.895946	–	7.446942×10^2	–	4.085428×10^4	–
256 × 256	2.649119×10^{-3}	10.0943	4.907694	7.2455	1.662587×10^2	7.9409
512 × 512	2.590272×10^{-4}	3.3543	4.386424×10^{-2}	6.8059	1.008079	7.3657
1024 × 1024	5.793892×10^{-5}	2.1605	3.933254×10^{-3}	3.4792	8.501939×10^{-3}	6.8896
2048 × 2048	6.983459×10^{-6}	3.0525	3.009321×10^{-4}	3.7082	3.740583×10^{-4}	4.5065

that the medium inside the ellipse is characterized by a constant wavenumber k_1 (typically, $k_1 > k_0$), and that at the interface Γ the solution and its first normal derivative are continuous, see formulae (6) and (19).

The exterior AP and its discretization remain the same as in Section 3.1, while the interior AP is formulated on the rectangle $[-a - 0.2, a + 0.2] \times [-b - 0.2, b + 0.2]$, where a and b are the major and minor semi-axes of the ellipse, respectively. We keep $a = 1.8$ and vary b between 0.9 and 0.15, which yields the aspect ratios between 2 and 12. The boundary conditions $u \in \mathcal{U}_1$ for the interior AP (see Section 2.1) are homogeneous Dirichlet at the two horizontal sides of the rectangle, and local Sommerfeld-type conditions (complex) at its two vertical sides. The latter guarantee a unique solvability of the interior AP (no resonances), see [18, Section 4.2] or [6, Section 5.2]. The interior AP is discretized by the compact scheme [18] with fourth order accuracy on a uniform in each coordinate direction Cartesian grid. It is then solved by a sparse direct linear solver built into MATLAB. To simplify the monitoring and analysis of the grid convergence, the grid dimensions for the interior and exterior AP are always kept the same, i.e., those two grids are refined synchronously. As in Section 3.1, the convergence is assessed by evaluating the maximum norm of the difference between the numerical solutions obtained on two consecutive grids. In this section it is done independently for the exterior and interior parts of the overall solution.

Tables 6 and 7 demonstrate the grid convergence for two particular sets of parameters. The convergence for other cases that we tried with piecewise constant k looks similar. In addition to showing the convergence data in Tables 6 and 7, we also

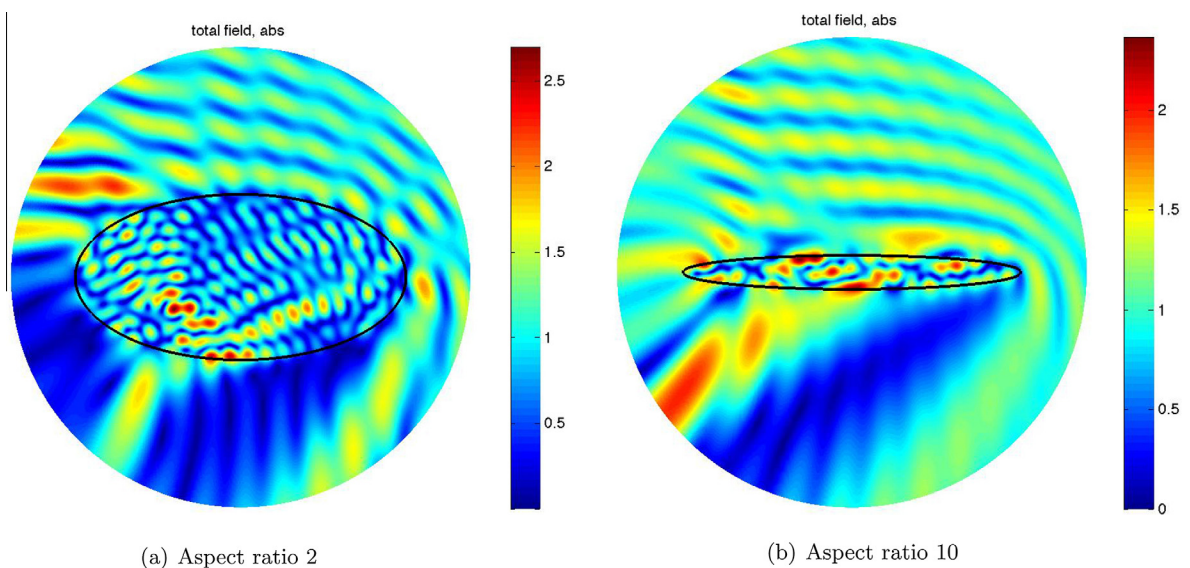


Fig. 6. Transmission and scattering of a plane wave with incidence angle 40° about an ellipse with $k_1 = 20$ (inside) and $k_0 = 10$ (outside). Absolute value of the total field is shown on the plots. The grid dimension is 1024×1024 for both the interior AP (Cartesian) and the exterior AP (polar).

Table 8

Transmission and scattering of a plane wave with incidence angle 40° about an inhomogeneous ellipse with aspect ratio 3 and interior wavenumber given by formula (55).

	$M = 44$ Exterior, $k_0 = 1$		$M = 43$ Exterior, $k_0 = 5$		$M = 70$ Exterior, $k_0 = 10$	
	$\ u^{(h)} - u^{(2h)}\ _\infty$	Conv. rate	$\ u^{(h)} - u^{(2h)}\ _\infty$	Conv. rate	$\ u^{(h)} - u^{(2h)}\ _\infty$	Conv. rate
<i>Ext. grid</i>						
128 × 128	1.342633×10^{-3}	–	3.189426×10^{-1}	–	2.273503	–
256 × 256	4.704559×10^{-5}	4.8349	2.112324×10^{-3}	7.2383	1.428778	0.6701
512 × 512	1.972406×10^{-6}	4.5760	1.037815×10^{-4}	4.3472	8.515279×10^{-3}	7.3905
1024 × 1024	1.128138×10^{-7}	4.1279	6.701632×10^{-6}	3.9529	4.664540×10^{-4}	4.1902
2048 × 2048	6.620319×10^{-9}	4.0909	5.703865×10^{-7}	3.5545	2.867676×10^{-5}	4.0238
	Interior, $k_1 = 3$		Interior, $k_1 = 15$		Interior, $k_1 = 30$	
	$\ u^{(h)} - u^{(2h)}\ _\infty$	Conv. rate	$\ u^{(h)} - u^{(2h)}\ _\infty$	Conv. rate	$\ u^{(h)} - u^{(2h)}\ _\infty$	Conv. rate
<i>Int. grid</i>						
128 × 128	3.067343×10^{-3}	–	1.043931	–	9.253122	–
256 × 256	6.693782×10^{-5}	5.5180	3.225823×10^{-2}	5.0162	2.960923	1.6439
512 × 512	1.396376×10^{-6}	5.5831	1.002967×10^{-4}	8.3292	4.859728×10^{-2}	5.9290
1024 × 1024	8.178574×10^{-8}	4.0937	6.580268×10^{-6}	3.9300	4.749737×10^{-4}	6.6769
2048 × 2048	5.333208×10^{-9}	3.9388	4.146442×10^{-7}	3.9882	2.935093×10^{-5}	4.0164

plot two of the solutions that we have computed, see Fig. 6. As the overall number of cases we have analyzed is large, we have chosen to plot different solutions compared to those presented in Tables 6 and 7.

3.3. Transmission/scattering problems with piecewise smooth coefficients

In this section, we keep the computational setting the same as in Section 3.2, except that we allow for a smooth variation of the wavenumber inside the ellipse:

$$k = \begin{cases} k_1 e^{-10(r-r_0)^6 r^6}, & \text{if } r \leq r_0, \\ k_1, & \text{if } r > r_0, \end{cases} \tag{55}$$

where $r = \sqrt{x^2 + y^2}$ and $r_0 = 1.6$. The variable coefficient Helmholtz equation is approximated with fourth order accuracy by the compact scheme of [18]. In Table 8, we show the results obtained for the ellipse with aspect ratio 3: $a = 1.8$ and $b = 0.6$. These results corroborate the design fourth order convergence rate of the algorithm in the case of variable coefficients.

4. Discussion

We have used the method of difference potentials combined with compact high order schemes to simulate a broad range of constant and variable coefficient 2D wave propagation problems for non-conforming boundaries/interfaces on regular structured grids. The method of difference potentials does not involve the evaluation of any singular integrals and offers automatic well-posedness of the equivalent boundary formulation of the problem. Our computations convincingly corroborate the design fourth order accuracy of the proposed methodology. We have also demonstrated a particular efficiency of our approach for computing scattering off a given fixed shape for multiple angles of incidence and various types of boundary conditions on the surface.

As of yet, we have computed solutions only for circular and elliptical boundaries. The case of general smooth boundaries was analyzed theoretically in [6, Appendix A], and the corresponding Taylor-based extension operators (Section 2.3) have been developed. Following this development, we will compute several transmission/scattering solutions for general smooth boundaries.

We will also extend this methodology from 2D to 3D. This will require that coordinates associated with a curve be replaced by surface-oriented coordinates [24]. Moreover, an efficient way of representing the traces $\xi_\Gamma^{(\Omega)}$ and $\xi_\Gamma^{(\Omega)}$ at the interface will need to be determined. The geometric partition of \mathbb{M}_0 into \mathbb{M}^+ and \mathbb{M}^- , see formula ((32)), is more complicated in 3D than in 2D. Iterative solvers with preconditioning seem to provide the only feasible approach in 3D for variable coefficients. Some possibilities include the iterative scheme of [19] which can be easily parallelized and the complex-shifted Helmholtz preconditioners to be inverted by multigrid, see [25,26].

In the future, we also plan to consider the case of layered media, analyze the solutions with singularities, and explore the possibility of extending the current methodology to time-dependent problems. As far as the latter, parabolic equations approximated by implicit schemes with accuracy $\mathcal{O}(\Delta t + \Delta x^2)$ were studied in [27].

References

- [1] A.N. Tikhonov, A.A. Samarskii, *Equations of Mathematical Physics*, Pergamon Press, Oxford, 1963.
- [2] A.P. Calderon, Boundary-value problems for elliptic equations, in: *Proceedings of the Soviet-American Conference on Partial Differential Equations in Novosibirsk*, Fizmatgiz, Moscow, 1963, pp. 303–304.
- [3] R.T. Seeley, Singular integrals and boundary value problems, *Am. J. Math.* 88 (1966) 781–809.
- [4] V.S. Ryaben'kii, Boundary equations with projections, *Russ. Math. Surv.* 40 (2) (1985) 147–183.
- [5] V.S. Ryaben'kii, *Method of difference potentials and its applications*, Springer Series in Computational Mathematics, vol. 30, Springer-Verlag, Berlin, 2002.
- [6] M. Medvinsky, S. Tsynkov, E. Turkel, The method of difference potentials for the Helmholtz equation using compact high order schemes, *J. Sci. Comput.* 53 (1) (2012) 150–193, <http://dx.doi.org/10.1007/s10915-012-9602-y>.
- [7] V.S. Ryaben'kii, V.I. Turchaninov, E.Y. Ėpshĕin, An algorithm composition scheme for problems in composite domains based on the method of difference potentials, *Comput. Math. Math. Phys.* 46 (10) (2006) 1768–1784.
- [8] V.S. Ryaben'kii, I.L. Sofronov, Difference potentials for the Helmholtz equation in exterior domains, *Appl. Numer. Math.* 33 (1–4) (2000) 533–540, [http://dx.doi.org/10.1016/S0168-9274\(99\)00122-1](http://dx.doi.org/10.1016/S0168-9274(99)00122-1).
- [9] J. Lonĕariĕ, V.S. Ryaben'kii, S.V. Tsynkov, Active shielding and control of noise, *SIAM J. Appl. Math.* 62 (2) (2001) 563–596, <http://dx.doi.org/10.1137/S0036139900367589>.
- [10] S.V. Tsynkov, On the definition of surface potentials for finite-difference operators, *J. Sci. Comput.* 18 (2) (2003) 155–189, <http://dx.doi.org/10.1023/A:1021111713715>.
- [11] D.S. Kamenetskii, Difference generalized Poincarĕ–Steklov operators and potentials with density from a space of jumps, *Comput. Math. Math. Phys.* 39 (8) (1999) 1275–1282.
- [12] D.S. Kamenetskii, On one form of representing the difference potentials, *Appl. Numer. Math.* 33 (1–4) (2000) 501–508, [http://dx.doi.org/10.1016/S0168-9274\(99\)00118-X](http://dx.doi.org/10.1016/S0168-9274(99)00118-X).
- [13] S.V. Utyuzhnikov, Generalized Calderĕn–Ryaben'kii's potentials, *IMA J. Appl. Math.* 74 (1) (2009) 128–148, <http://dx.doi.org/10.1093/imamat/hxn025>.
- [14] E. Kansa, U. Shumlak, S. Tsynkov, Discrete Calderon's projections on parallelepipeds and their application to computing exterior magnetic fields for FRC plasmas, *J. Comput. Phys.* 234 (2013) 172–198, <http://dx.doi.org/10.1016/j.jcp.2012.09.033>.
- [15] V.S. Ryaben'kii, Difference potentials analogous to Cauchy integrals, *Russ. Math. Surv.* 67 (3) (2012) 541–567.
- [16] A.M. Lyapunov, *Collected works of academician A.M. Lyapunov*, Wright–Patterson air force base: translation division, vol. 1 and 2, Foreign Technology Division, Dayton, OH, United States, 1967.
- [17] S. Britt, S. Tsynkov, E. Turkel, A compact fourth order scheme for the Helmholtz equation in polar coordinates, *J. Sci. Comput.* 45 (1–3) (2010) 26–47, <http://dx.doi.org/10.1007/s10915-010-9348-3>.
- [18] S. Britt, S. Tsynkov, E. Turkel, Numerical simulation of time-harmonic waves in inhomogeneous media using compact high order schemes, *Commun. Comput. Phys.* 9 (3) (2011) 520–541, <http://dx.doi.org/10.4208/cicp.091209.080410s>.
- [19] E. Turkel, D. Gordon, R. Gordon, S. Tsynkov, Compact 2D and 3D sixth order schemes for the Helmholtz equation with variable wave number, *J. Comput. Phys.* 232 (1) (2013) 272–287, <http://dx.doi.org/10.1016/j.jcp.2012.08.016>.
- [20] A. Bayliss, M. Gunzburger, E. Turkel, Boundary conditions for the numerical solution of elliptic equations in exterior regions, *SIAM J. Appl. Math.* 42 (2) (1982) 430–451, <http://dx.doi.org/10.1137/0142032>.
- [21] A.A. Reznik, Approximation of surface potentials of elliptic operators by difference potentials, *Dokl. Akad. Nauk SSSR* 263 (6) (1982) 1318–1321.
- [22] J.J. Bowman, T.B.A. Senior, P.L.E. Uslenghi (Eds.), *Electromagnetic and Acoustic Scattering by Simple Shapes*, A Summa Book, Hemisphere Publishing Corporation, New York, 1987.
- [23] S. Britt, S. Tsynkov, E. Turkel, A high order numerical method for the Helmholtz equation with non-standard boundary conditions, *SIAM J. Sci. Comput.*, submitted for publication.
- [24] E.H. Hirschel, W. Kordulla, *Shear flow in surface-oriented coordinates*, Notes on Numerical Fluid Mechanics, vol. 4, Friedr. Vieweg & Sohn Verlagsgesellschaft mbH, Braunschweig/Wiesbaden, 1981–1986.
- [25] Y.A. Erlangga, C. Vuiik, C.W. Oosterlee, On a class of preconditioners for solving the Helmholtz equation, *Appl. Numer. Math.* 50 (3–4) (2004) 409–425, <http://dx.doi.org/10.1016/j.apnum.2004.01.009>.
- [26] Y. Erlangga, E. Turkel, Iterative schemes for high order compact discretizations to the exterior Helmholtz equation, *Math. Model. Numer. Anal. (ESAIM: M2AN)* 46 (2012) 647–660, <http://dx.doi.org/10.1051/m2an/2011063>.
- [27] Y. Epshteyn, Algorithms composition approach based on difference potentials method for parabolic problems, *Commun. Math. Sci.*, submitted for publication.